Final Technical Report

Agency: DOE/EERE/Advanced Manufacturing Office

Award Number: DE-EE0007868

Recipient Organization: Purdue University

Project Title: High-Silicon Steel Strip by Single-Step Shear Deformation Processing

Principal Investigator: Srinivasan Chandrasekar

Co-Principal Investigators: Kevin Trumble, Purdue University
James Mann, M4 Sciences LLC
Aashish Rohatgi and Mert Efe, Pacific Northwest National Labs

Project Period: 06/15/2017 – 06/14/2022

Partners: M4 Sciences LLC and Pacific Northwest National Labs

DOE Technology Manager: Stephen Sikirica
DOE Project Officer: Gibson Asuquo
DOE Project Monitor: Colleen Lipps/John Harrington
DOE Grants Specialist: Melissa Jacobi

Acknowledgment: This material is based upon work supported by the U.S. Department of Energy's Office of Energy Efficiency and Renewable Energy (EERE) under the Advanced Manufacturing Office (AMO) Award Number DE-EE0007868.

Disclaimer: This report was prepared as an account of work sponsored by an agency of the United States Government. Neither the United States Government nor any agency thereof, nor any of their employees, makes any warranty, express or implied, or assumes any legal liability or responsibility for the accuracy, completeness, or usefulness of any information, apparatus, product, or process disclosed, or represents that its use would not infringe privately owned rights. Reference herein to any specific commercial product, process, or service by trade name, trademark, manufacturer, or otherwise does not necessarily constitute or imply its endorsement, recommendation, or favoring by the United States Government or any agency thereof. The views and opinions of authors expressed herein do not necessarily state or reflect those of the United States Government or any agency thereof.

DOCUMENT AVAILABILITY

Reports produced after January 1, 1996, are generally available free via the U.S. Department of Energy (DOE) Information Bridge.

Web site http://www.osti.gov/bridge

Reports produced before January 1, 1996, may be purchased by members of the public from the following source.

National Technical Information Service
5285 Port Royal Road
Springfield, VA 22161
Telephone 703-605-6000 (1-800-553-6847)
TDD 703-487-4639
Fax 703-605-6900
E-mail info@ntis.gov
Web site http://www.ntis.gov/support/ordernowabout.htm

Reports are available to DOE employees, DOE contractors, Energy Technology Data Exchange (ETDE) representatives, and International Nuclear Information System (INIS) representatives from the following source.

Office of Scientific and Technical Information
P.O. Box 62
Oak Ridge, TN 37831
Telephone 865-576-8401
Fax 865-576-5728
E-mail reports@osti.gov
Web site http://www.osti.gov/contact.html

List of Acronyms

ASTM – American Society of Testing Materials
HCE – Hybrid Cutting-Extrusion
FM – Free Machining
CR – cold rolling
RD – rolling direction
VIM – Vacuum Induction Melting
EDM – Electro-Discharge Machining
DIC – Digital Image Correlation
UFG – ultrafine grained
EBSD – Electron Back Scattered Diffraction
AC – alternating current
DC – direct current

Table of Contents

Executive Summary

HIGH-SILICON STEEL SHEET BY SINGLE STAGE SHEAR-BASED PROCESSING

Srinivasan Chandrasekar and Kevin P. Trumble (Purdue University);
James B. Mann (M4 Sciences LLC); Aashish Rohatgi and Mert Efe (PNNL)

Additional contributions from Stiven Puentes Rodriguez, Anirudh Udupa, Mohammed Issahaq, Mojib Saei and Debapriya Mohanty (Purdue University); and supplementary inputs/guidance from tool and metals manufacturers

It is well known that Fe-Si alloys with Si content higher than in conventional electrical sheet steels (>3.2% Si) can make a significant impact in improving the efficiency of electrical motors if they are available in sheet/foil (strip) forms at suitable cost. While the magnetic and electrical attributes (e.g., resistivity, core loss) of these high-Si Fe alloys, of relevance to electrical motor core laminations, are known to be exceptional, the alloys have limited workability, making them difficult to produce consistently in sheet/foil (strip) forms. Current processing techniques such as rolling, while adequate for producing conventional electrical steel sheet, do have important disadvantages - large energy consumption and emissions, limitations in processing of low-workability alloys (e.g., high-Si content steels), large-scale plant infrastructure, and less than adequate capability to engineer sheet metals with specific microstructures (e.g., fine-grained) and crystallographic textures (e.g., shear textures). It is therefore of interest to have an alternative commercial process that can produce sheet/foil (strip) from high-Si Fe alloys and which can also overcome some of the deficiencies of current multistage strip processes.

The goal of the present project was design and demonstration of a new energy-efficient pilot process for producing high-Si electrical steel strip of commercial widths and thickness, and with superior electrical and magnetic properties than current electrical steels (Fe-3.2% Si as benchmark). The applications domain for these steels is electrical motor core laminations. We have addressed this goal by accomplishment of the following specific objectives and tasks outlined in the SOPO.

a) Development of an Fe-4Si-4Cr alloy with electrical resistivity > 80 μΩ-cm, induction flux density > 1.48 T at 5000 A/m and core loss 35% lower than the benchmark 3.2% Si alloy). The alloy which meets DOE target specifications for motor core attributes was designed with the Si content controlled for the electrical properties and the Cr content tailored to meet material/process workability requirements.
b) A unique machining-based deformation processing system was designed and scaled-up to produce strip of commercial width (25 mm to 150 mm) and thickness (up to 0.5 mm) from the Fe-4Si-4Cr alloy and other alloys of varied workability including copper, Al6061-T6 and naval brass. The key attributes of the machining-based strip production are deformation processing by concentrated simple-shear; single-step production of strip from ingot using compact machine infrastructure; strip surface finish of Ra 0.35 to 1 micrometer that is comparable/superior to that of rolled strip; discrete production of strip that can potentially be done at point of use; and controllability of strip mechanical/formability properties by deformation control.

c) The electrical, magnetic, surface quality, mechanical, formability, and metallurgical properties/attributes of the machining-based strip were established by direct ASTM standard or equivalent measurement techniques.
d) Punching characteristics of the strip in terms of load, edge quality and macro defects were similar to those of conventional 3.2% Si electrical steels. These punching characteristics are critical from a manufacturability perspective for motor/transformer core applications.
e) A modeling framework for energy analysis of multistage rolling and the machining-based deformation processing has been established. Application of this modeling to the two strip-processes showed that the machining-based process requires significantly lower specific energy for processing, ~ 25% of that for rolling. The modeling framework can be adapted for a range of sheet-metal forming, bulk metal forming, and machining processes. It can be used to identify key parameters controlling process specific energy.
f) A comparative analysis of advantages and disadvantages of machining-based processing against rolling for strip production.

The single stage machining-based processing, with compact infrastructure, represents a new manufacturing paradigm for sheet and foil manufacturing that can potentially also be applied to advanced titanium, aluminum, copper and magnesium alloys.

The goals and objectives were accomplished by a cross-disciplinary project team comprising of personnel from Purdue University; M4 Sciences LLC, a small-business focused on advanced manufacturing technology development; the Pacific Northwest National Labs; and tool manufacturers. The team is currently in advanced discussions with multiple entities for future process development for commercialization.

1. Introduction

It is well known that Fe-Si alloys with Si content higher than in conventional electrical sheet steels (>3% Si) can make a significant impact in improving the efficiency of electrical motors if they are available in sheet/foil (strip) forms at suitable cost. While the magnetic and electrical attributes (e.g., resistivity, core loss) of these high-Si Fe alloys, of relevance to electrical motor core laminations, are known to be exceptional, the alloys have limited workability, making them difficult to produce consistently in sheet/foil (strip) forms. Current processing techniques such as rolling, while adequate for producing conventional electrical steel sheet, do have important disadvantages – large energy consumption and emissions, limitations in processing of low-workability alloys (e.g., high Si content steels), large-scale plant infrastructure, and less than adequate capability to engineer sheet metals with specific microstructures (e.g., fine-grained) and crystallographic textures (e.g., shear textures). The large energy consumption of the rolling process is a direct consequence of its multistage nature, see **Fig. 1.1** (left), involving multiple energy-intensive hot rolling and workpiece pre-heating steps (for workability and large thickness reductions) coupled with cold-rolling steps to achieve product properties. It is therefore of commercial interest to have an alternative process that can produce sheet from high-Si Fe alloys and that can also overcome some of the deficiencies of the rolling process.

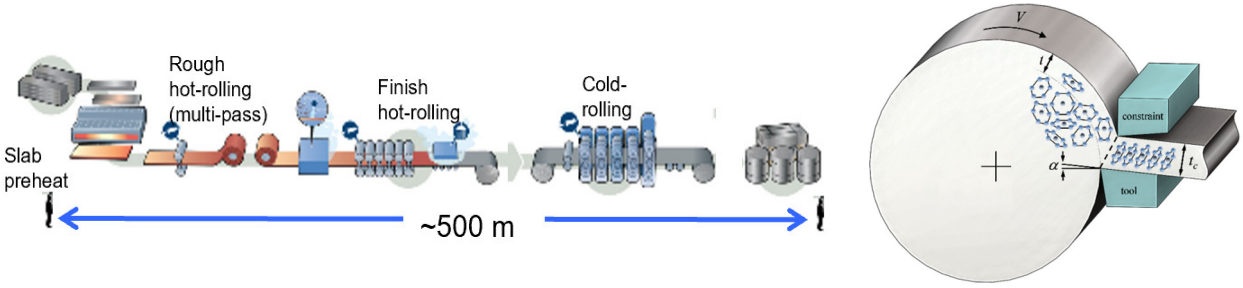

Figure 1.1 (Left) Schematic of typical rolling plant for production of sheet metals involving multiple stages of processing. (Right) Single-stage production of strip by machining-based deformation processing (project focus); in this process, the chip created by shear deformation is the strip product of thickness (t_c).

Project Goals/Objectives The present project is an attempt to develop an economically viable and energy efficient process for making electrical steel sheet that is applicable to a wide range of Fe-Si alloys, including the very high Si content steels (e.g., Fe-6.5% Si), and to other alloys of limited workability. The machining-based deformation processing (**Fig. 1.1,** right) seeks to produce strip by chip formation, where the chip is the strip (sheet/foil) product. It is a single-stage deformation process wherein the strip is produced by intense local shear-deformation that is controllable via tool and deformation zone geometry design. With compact infrastructure and much lower energy requirements than rolling, as shown in this project, the process is applicable for sheet production from a range of alloys. The project goal is to demonstrate a production system that can provide high-Si electrical sheet of commercial width (> 25 mm) and thickness (up to 0.5 mm), with superior electromagnetic properties, from which motor laminations can be stamped out using standard stamping methods. The laminations can then be incorporated into standard motor designs and the motor performance characterized. At the project core is design, construction and demonstration of

a new sheet-processing system. It is envisaged that the sheet production process will be applicable to the entire spectrum of low-workability alloys, even beyond electrical steels.

The specific project objectives are,

a) Fe-Si alloy development with selected additions of Al, Mn and Cr for meeting combination of electromagnetic properties and workability favorable for machining-based processing of sheet/foil (strip). This is for screening possible workpiece alloy materials for the latter stages of the project that focus on scale-up of sheet making.
b) Characterize mechanics and materials aspects of the deformation processing, including interactive effects of large-strain deformation (e.g., strain, temperature, strain path) on structure and properties of the sheet metal.
c) Scale up the machining (shear-based) deformation processing to enable strip production from alloys that model the workability of the high Si content (>3.2 wt%) Fe-Si electrical steel, such as Fe-4Si-4Cr, Al 6061-T6, and naval brass.
d) Develop machine/process and large-scale tooling design to achieve the scale-up both in terms of strip width (25 mm to 150 mm) and thickness (up to 0.5 mm)
e) Apply the new process to high-Si, low-loss electrical steels. The specific steel selection is based on the alloy development to meet property specifications.
f) Enable high-Si electrical steel sheet production for increased-efficiency electric motors.
g) Characterize properties of the electrical steel sheet of relevance for motor applications, and manufacturability of motor laminations.
h) Modeling and analysis of energy consumption in sheet production by rolling and the machining-based processing; and establish comparative benefits.

The layout of the report, comprised of 10 sections, is as follows. Section 1 is the Introduction including project objectives. Sections 2 to 5 discuss alloy development, machining-based deformation processing and equipment design, production of strip using the newly developed process system, and characterization of magnetic properties of strip. Section 6 presents a full-scale energy analysis of rolling and machining-based processing, and makes comparative conclusions. Section 7 addresses manufacturability characteristics of the strip for motor core laminations. Section 8 summarizes the key project findings, and outlines future work towards commercialization of the process. Section 9 provides a listing of products resulting from the project and Section 10 is a bibliography of literature related to the project.

2. High-Resistivity Electrical Steel – Development of an Experimental Alloy

The objective with regard to alloy development was an Fe-Si-X ternary alloy that could meet the DOE electrical property requirements for high-efficiency motor core materials, while having sufficient workability to be processed into strip by the machining-based processes. The alloy development was guided by the fact that while the Fe-6.5%Si alloy is the best material for the electrical power applications domain based purely on electrical property considerations (e.g., resistivity, core loss), its workability is too limited to be processed into sheet forms by deformation processing routes. Furthermore, the punching characteristics of the alloy are also deemed to be unsuitable for motor core laminate production. The objective was thus to obtain an alloy with the

high resistivity of Fe-6.5Si (at least 80 μΩ·cm), but with sufficient workability for sheet production and punching.

Several Fe-Si-X ternary alloys were assessed based on their phase diagrams, and compositional effects on resistivity and workability. Following this assessment, two specific alloy systems were selected for further study. These were Fe-3Si-3Al and Fe-4Si-4Cr (wt%). While both alloys met specifications on resistivity (>80 μΩ-cm), the Cr-containing alloy was finally chosen over the Al-containing alloy as the experimental alloy system for the project on the basis of a) its higher workability, and b) the known difficulties with high-Al content materials in steelmaking and hot-working. The Fe-4Si-4Cr alloy provided the desired resistivity, with (potentially) sufficient workability for deformation processing and punching (established subsequently in the course of the project). We detail this alloy selection in this section.

The dramatic effect of Si on the loss of ductility in iron is well known. In general, this poor ductility (workability) above about 4% Si has been attributed to a B2 ordering due to the dissociation of superlattice dislocations induced by the high Si amounts in the material. Silicon is the most potent alloying element to increase the electrical resistivity of iron. However, other elements like aluminum and chromium are also effective alternatives. Moreover, Fe-Al and Fe-Cr phase diagrams show that other than the gamma loop typical of iron alloys, there is no other type of ordering or phase transformation up to 10 wt% for the Fe-Al system and more than 20 wt% for the Fe-Cr system. In fact, previous studies have demonstrated that if the correct thermomechanical procedure is followed (hot rolling down to 1 mm + cold rolling), thin sheet of Fe-Si-Al alloys can be produced. However, there is no solid agreement about how much Si+Al can be added while still maintaining good cold workability, i.e., before the alloy gets too brittle. Some authors have claimed that Si+Al has to be lower than 3.5 wt%, while others have suggested that even Fe-6.5(Si+Al) is possible if the correct procedure is followed. Information about the workability of alloys in the Fe-Si-Cr system is limited, as is any type of resistivity information about this alloy.

2.1 Experimental methods

2.1.1 Materials for alloy selection experiments

Fe-3Si-3Al and Fe-4Si-4Cr (wt%) samples were produced in-house in order to control the purity of the alloy. The rationale for their selection is discussed fully in a recent Ph.D thesis from our group [B. S. Puentes-Rodriguez, PhD Thesis, Purdue University, 2022]. High purity elemental metals used to manufacture the alloys had compositions in wt.% as follows: Fe 99.98%, Si (>99.999%), Cr 99%, and Al 99.99%. The experimental alloys were made using an arc melter with a non-consumable tungsten electrode on a water-cooled copper hearth. The alloys were first melted under flowing 99.99% Ar, and then were turned over and re-melted three times to obtain button shaped samples with good homogeneity. The button samples were approximately 50 g, diameter of 4 cm, and thickness of 1.5 cm approximately. The buttons were hot rolled to ~1 mm thickness, and then cold rolled down to the limit of the mills (~200 μm) to produce thin strips ~10 mm wide. The samples were heated in a box furnace in air up to 800 °C for 10 min before the first pass and in between all the passes during hot rolling. Samples were polished after hot rolling and before cold rolling to remove the small amount of oxidation.

2.1.2 Materials for workability experiments

Fe-3.2Si and Fe-1Si wt% materials were obtained from AK Steel and Nucor in the as-hot rolled and the as-cast conditions, respectively, for baseline comparisons. The Fe-4Si-4Cr alloy for the

workability experiments was manufactured and obtained in the as-cast condition from Sophisticated Alloys Inc, Butler, Pa. The manufacturing of this ingot was done as per specifications outlined by the project team. An ingot of 4.3 in diameter and height of 11.5 in (plus hot top) was prepared by Vacuum Induction Melting (VIM); the chemical analysis reported 4.02%Si, 3.88%Cr, and interstitials (C, O, and S) < 100 ppm. The Fe-6.5Si wt% was produced in-house via arc melting with a non-consumable tungsten electrode on a water-cooled copper hearth, using high purity elemental metals Fe (99.98%) and Si (>99.999%). Specimens of each material were manufactured with a geometry of 12 mm width and 8 mm thickness. These specimens were then hot rolled at 800 °C to a thickness close to 2 mm using a Stanat rolling mill with 5 in diameter rolls. The specimens were cold rolled to 0.5 mm with progressive reductions of 5%. After every step, specimens were checked for presence of cracks, ripples, or other typical defects in the rolling process.

For metallographic preparation, the as-cast buttons were cut using a wire EDM and the rolled strips were cut with a low-speed diamond saw. Silicon carbide paper with grits from 320 to 2000 were used to grind the samples, with a final polishing using 0.05 μm alumina powder dissolved in water and 0.02 μm colloidal silica. The samples were etched for microstructure examination using 5% nital for the Fe-Si alloys and 40% nitric acid aqueous solution for the Fe-4Si-4Cr alloy. Vickers hardness testing was performed with a load of 500 g (HV0.5) and at least 250 μm distance between indentations. At least 10 indentations were made for each hardness and the values are reported as the mean ± one standard deviation.

2.1.3 Resistivity

Resistivity measurements were done using the 4-wire method of ASTM A712-14 Standard Test Method for Electrical Resistivity of Soft Magnetic Alloys. A multimeter (HP 3468B) measured the resistance of Fe-3Si-3Al and Fe-4Si-4Cr (wt%) strips with a resolution of 1 mΩ, and the geometry of the strip was measured with a Vernier caliper with a resolution of 0.01 mm. Three measurements at 5 cm, 10 cm, and 14 cm length were taken for each strip. The results showed that the resistivity values were similar to that measured with a 25 cm length standard sample.

2.2 Alloy selection

In power transformation devices like electric motors and magnetic transformers, core losses are composed of eddy current losses, hysteresis losses, and anomalous losses. Eddy current losses are frequency dependent and can be reduced by increasing electrical resistivity, most effectively through solid solution alloying additions. Whereas hysteresis losses are affected also by microstructure modifications such as grain size, and texture. At frequencies of approximately 50 Hz, the ratio of hysteresis losses and eddy current losses is close to 1:1. The higher the frequency, the higher the eddy current losses compared to the hysteresis losses. The eddy current losses become the predominant source of energy loss in high-frequency applications (above traditional 50-60 Hz), thus the importance of electrical resistivity.

Figure 2.1 shows the effect of different alloying elements on the electrical resistivity of iron. Silicon has the greatest effect. As shown in the figure, aluminum and chromium are good options to be used as partial substitutes of Si. This elemental substitution was optimized to obtain an alloy with outstanding magnetic performance, but with improved workability as opposed to Fe-6.5Si wt%. The idea of using Al and Cr as a substitute of Si comes from the fact that these two elements have significant effect on the electrical resistivity of Fe, which is a key parameter to control eddy

current loses especially at high frequency applications. Concurrently, their strengthening effect on Fe is rather low compared to Si.

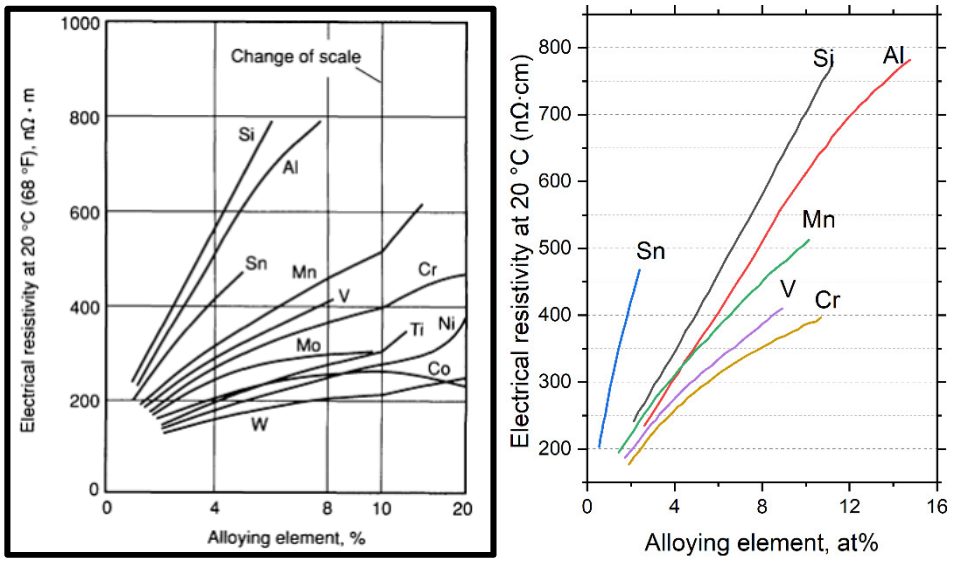

Figure 2.1 Effect of alloying elements on electrical resistivity of Fe. Left) alloying elements in wt% (ASM Handbook, Vol. 2). Right) adaptation showing alloying element in at%.

The selection of the alloys was based on resistivity calculations as a function of their composition, with a targeted resistivity of at least 80 μΩ·cm, which corresponds to the high resistivity of Fe-6.5Si wt%. Another constraint was to keep Fe at% as high as possible, since this is what determines the flux density saturation. To estimate a tentative alloy composition, a model developed by AK Steel (US Patent 7,140,417 B2, 2006) was used to predict electrical resistivity electrical steels according to Eq. 2-1.

$$\rho = 13 + 6.25(\%\,Mn) + 10.52(\%Si) + 11.82(\%Al) + 6.5(\%Cr) + 14(\%\,P) \qquad (2\text{-}1)$$

where ρ is the electrical resistivity with units of μΩ·cm, and the compositions are in wt%. Based on this model, the following two compositions are proposed:

- Fe-3Si-3Al wt% with an estimated $\rho = 80$ μΩ·cm based on Eq. 2-1
- Fe-4Si-4Cr wt% with an estimated $\rho = 81$ μΩ·cm based on Eq. 2-1

Experimental alloy ingots were cast in a 2-kg vacuum induction melting (VIM) furnace (Balzers, Germany). The elemental metals were melted in alumina crucibles (Zircoa). The furnace was evacuated and backfilled with Ar. The melts were heated to ~ 1550 °C and poured into a copper mold producing ingots of 50 mm in diameter and 20 mm thick.

Figure 2.2 shows the VIM ingots and the as-cast structure of the two experimental alloys. Columnar grains can be seen in both samples but there is no presence of dendritic structure. The absence of dendritic structure is likely due to the narrow freezing range of these alloys and high solidification rate in the VIM. One thing to highlight is the absence of secondary phases or inter-

granular phases, which is good since these are detrimental to the alloy workability. The presence of just one phase allows for hot rolling the sample right after casting with no homogenization needed. Hardness measurements on the as-cast alloys gave values of 259 ± 11 HV0.5 and 233 ± 11 HV0.5 for the Fe-3Si-3Al and Fe-4Si-4Cr, respectively. Previous studies had suggested that Cr has little effect on strengthening of Fe alloys, and this is corroborated by the fact that the Fe-3Si-3Al hardness is higher than the Fe-4Si-4Cr despite the fact the Cr alloy has more Si content. Also, this hypothesis is supported by the fact that the Fe-4Si-4Cr hardness is similar to that reported for Fe-4Si wt%. The lack of solution strengthening is a good indication that Cr does not affect the workability of Fe.

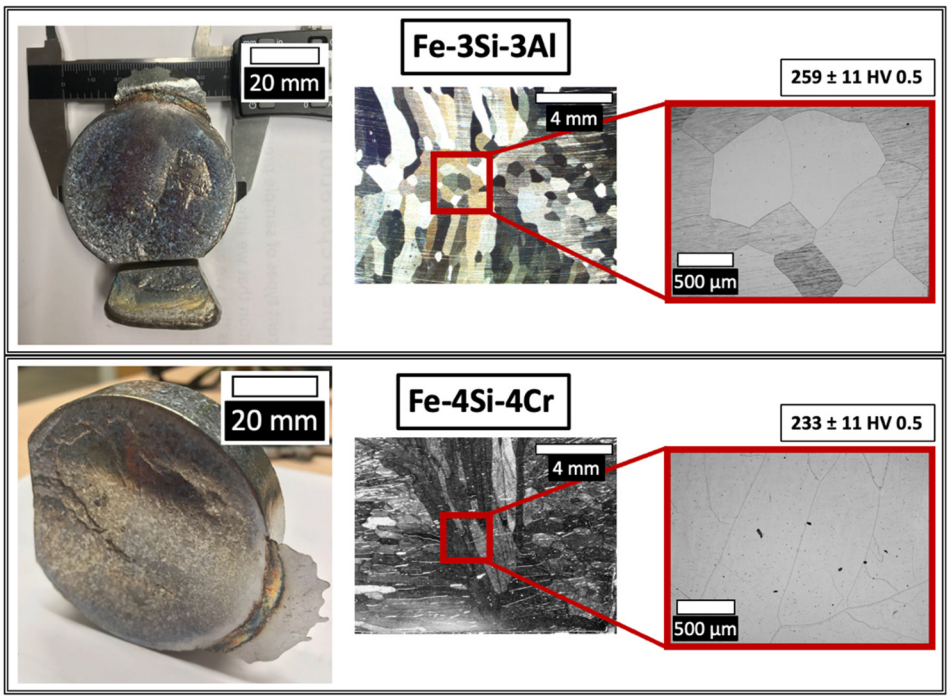

Figure 2.2 In-house made VIM ingots, experimental alloys as-cast micro and macro structure, and hardness. Top) Fe-3Si-3Al. Bottom) Fe-4Si-4Cr.

Preliminary cutting experiments were carried out with both the experimental alloys. Both alloys exhibited similar machinability based on force measurements, see **Fig. 2.3** below.

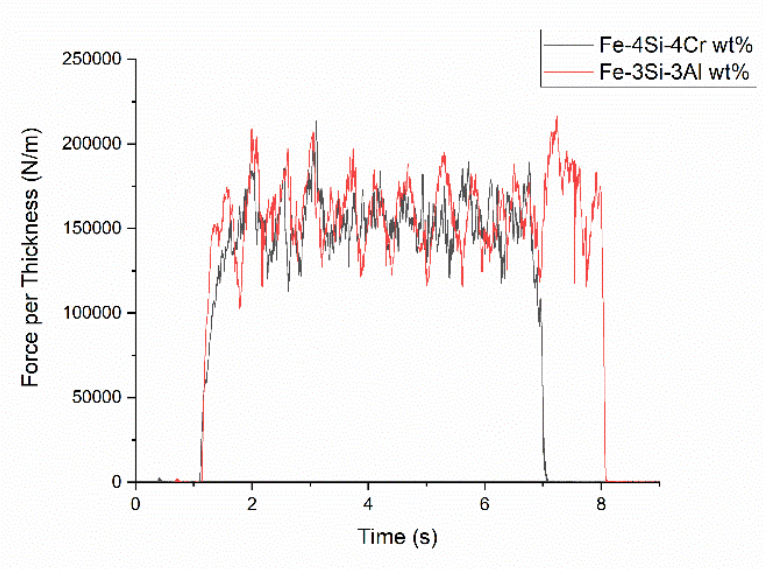

Figure 2.3 Specific cutting forces in free machining (FM) for the Fe-4Si-4Cr and Fe-3Si-3Al.

2.3 Electrical resistivity results

The resistivities measured over the three different lengths were **74 ± 3 μΩ·cm for Fe-3Si-3Al wt% and 85 ± 3 μΩ·cm for Fe-4Si-4Cr wt%**. The standard deviation is below 5% of the average resistivity. The target resistivity was at least 80 μΩ·cm based on the resistivity of Fe-6.5Si wt%. Resistivity measurements for Fe-3Si-3Al wt% stayed below the target. On the other hand, the Fe-4Si-4Cr alloy showed a resistivity higher than the targeted value of 80 μΩ·cm, meeting the alloy target (DOE) specification. Equation 2-1 predicts Fe-4Si-4Cr wt% should have a resistivity of 81 μΩ·cm somewhat lower than what was realized in the experiments.

2.4 Experimental alloy workability

Since Fe-4Si-4Cr alloy has higher electrical resistivity (meeting target requirements), lower hardness, and similar cutting forces than the Fe-3Si-3Al alloy, it was decided that Fe-4Si-4Cr would be the experimental alloy used to complete the study. From here onwards, this Fe-4Si-4Cr alloy will be called the experimental alloy. All of the deformation processing and property characterization will focus on this alloy.

Commercial production of non-oriented electrical steel sheets is composed of a series of complex steps. **Figure 2.4** shows a typical commercial sheet (conventional) processing schedule. The workability of the material is an extremely important parameter for all rolling steps of this process schedule. We therefore use rolling as the basis for analyzing the workability of this experimental alloy.

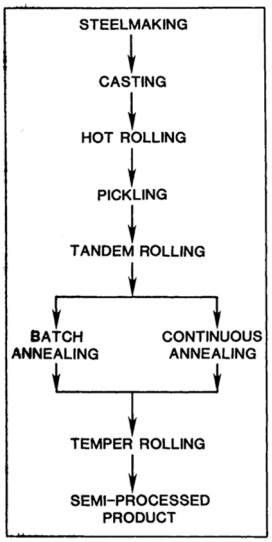

Figure 2.4 Commercial electrical steel production steps (with permission, Springer).

Workability of the experimental alloy was assessed by replicating the commercial rolling process, albeit on a smaller scale. For this experiment, the Fe-4Si-4Cr experimental alloy is compared to traditional Fe-Si alloys, Fe-1Si, Fe-3.2Si, and Fe-6.5Si wt%. Samples were hot rolled and subsequently cold rolled. **Figure 2.5** shows the results obtained from this workability experiment. The experimental alloy, the Fe-1Si and the Fe-3.2Si alloys could all withstand 75% cold work. It was possible to obtain 0.5 mm thick strips of these alloys, without visible cracks or defects along the strip edges. In contrast, the Fe-6.5 Si alloy failed even during hot rolling (**Fig. 2.6**).

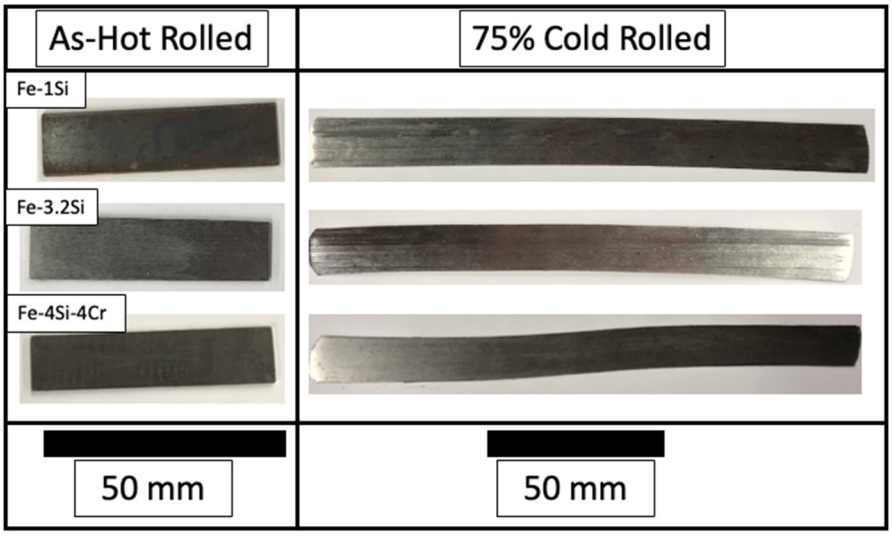

Figure 2.5 Workability test results after 75% cold work reduction: results for Fe-1Si, Fe-3.2Si, and Fe-4Si-4Cr alloys.

These results showed that despite the high silicon content, the experimental alloy was cold-rollable in contrast to the Fe-6.5Si wt% that possess a similar resistivity. Hence, this Fe-4Si-4Cr alloy was down selected as a suitable experimental alloy for the project.

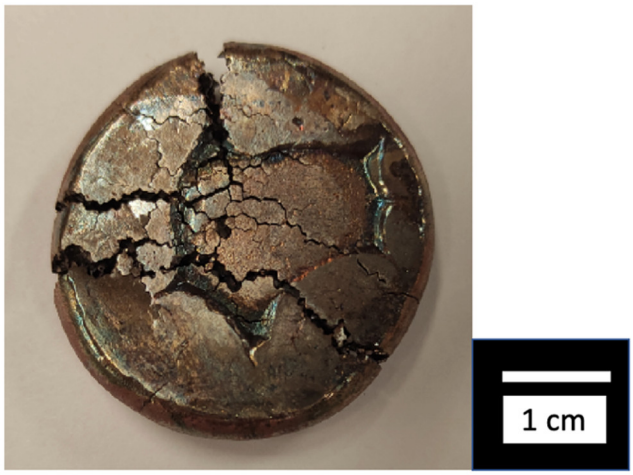

Figure 2.6 Fe-6.5Si wt% sample failing after only 5% reduction during hot rolling.

Previous studies had suggested that Cr has little effect on strengthening of Fe alloys, and this is corroborated by the fact that the Fe-3Si-3Al hardness is higher than the Fe-4Si-4Cr despite the fact the Cr alloy has more Si content. Also, this hypothesis is supported by the fact that the Fe-4Si-4Cr hardness is similar to that reported for Fe-4Si wt%. The lack of solution strengthening is a good indication that Cr does not affect the workability of Fe.

3. Machining-Based Deformation Processing of Electrical Steel

In this section, we describe production of electrical steel strip from the Fe-4Si-4Cr experimental alloy using two machining-based deformation processes – Free M(FM) followed by a light cold rolling step (FM + CR process); and (constrained) Hybrid Cutting-Extrusion process (HCE process). Both of these processes have shown promise to produce strip and sheet from low-workability alloys because of the unique controllability of deformation parameters.

3.1 Mechanics of strip production by FM and HCE

Figure 3.1 is a schematic of strip production by chip formation via free machining (FM), under plane strain conditions. In this rotary configuration, a workpiece is rotating at constant surface velocity V_0. A sharp cutting tool with rake angle α engages the rotating workpiece at a preset depth t_0, the undeformed chip thickness. As the cutting tool engages the workpiece, a continuous chip of metal with deformed chip thickness t_c is produced. Typically, t_c is greater than t_o because of the deformation. The chip constitutes the strip product. An analogous linear configuration of the FM (and the HCE) is also used in the present study wherein the strip cutting resembles a planing process. The chip forms by intense and localized shear that occurs within a narrow deformation

(process) zone AB. This deformation zone can be idealized as a shear plane due to its small width of ~100 µm. The strip surface in face in contact with the cutting tool (rake face) is quite smooth, with minimal roughness, since the surface is fully constrained by contact with the tool. The roughness on this surface is, as we shall see, comparable or superior to that of rolled strip. In contrast, the material along the upper surface face of the strip wherein there is no constraint, can flow normal to the surface of the strip. As a result, the top free surface of the strip develops some roughness. The FM strip can be lightly rolled in order to make the free surface roughness also comparable to that of conventional rolled sheet, as depicted in Fig. 3.1(b).

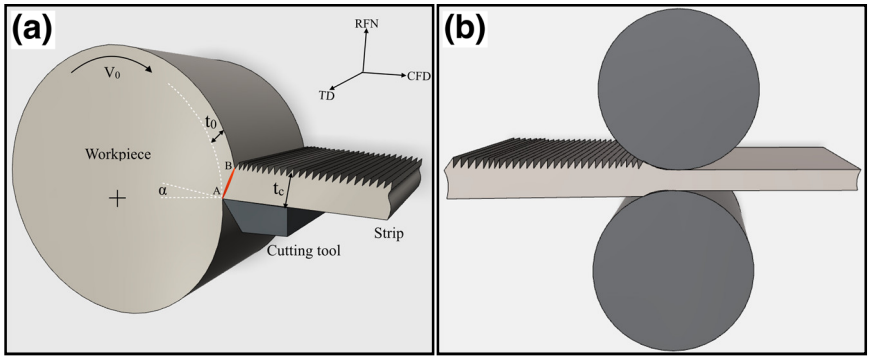

Figure 3.1 (a) Schematic of FM + CR process showing strip production using a rotary configuration. CFD is chip (strip) flow direction, and ND is the direction normal to the strip surface. (b) Light cold-rolling can be applied to smooth the free surface roughness of the strip.

Figure 3.2 shows a schematic of the hybrid cutting-extrusion (HCE) process for strip. The process and deformation configuration are broadly similarly to that of the FM, except for the addition of a constraining tool/die located directly across from the primary cutting tool. As with the FM, both rotary and linear configurations of the process can be configured for strip production. The use of the constraining tool in the HCE enables the strip thickness (t_c) at the exit of the deformation zone to be controlled *a priori.* In the HCE, t_c can even be set much smaller than t_o unlike in FM, enabling very large plastic strains and hydrostatic pressures to be imposed simultaneously in the deformation zone.

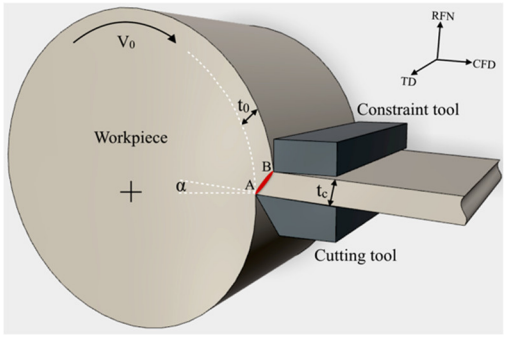

Figure 3.2 Schematic of strip production by hybrid cutting-extrusion (HCE).

The large hydrostatic pressure, intense/localized shear strain, and adiabatic deformation heating in the FM and HCE provide shear deformation conditions that are favorable for suppression of cracking in low workability alloys – an outstanding feature of this type of processing for strip production. Furthermore, these deformation parameters can be controlled via the process variables as shown in the ensuing. In both the FM and the HCE, the critical parameters controlling deformation strain are the chip (strip) thickness ratio $\lambda = \frac{t_c}{t_0}$ and the tool rake angle α. The HCE allows for even greater control of the deformation than the FM, because of the exit constraint and *a priori* control of t_c.

3.2 Process deformation conditions and control

Digital image correlation (DIC) analysis of material flow in the process zone utilizing high-speed imaging shows that the shear deformation in this zone is indeed intense and highly confined, see **Fig. 3.3.** This strain rate field also shows control of the deformation path which determines the crystallographic texture in the strip. Because of the small width/thickness of the deformation zone, it is reasonable to idealize it as a shear plane (shear plane model). Consequently, the effective strain imposed in the strip can be estimated as:

$$\varepsilon = \frac{1}{\sqrt{3}}\left(\frac{\lambda}{cos(\alpha)} + \frac{1}{\lambda\, cos(\alpha)} - 2\, tan(\alpha) \right) \qquad (3\text{-}1)$$

where $\lambda = \frac{t_c}{t_0}$ is the chip (strip) thickness ratio.

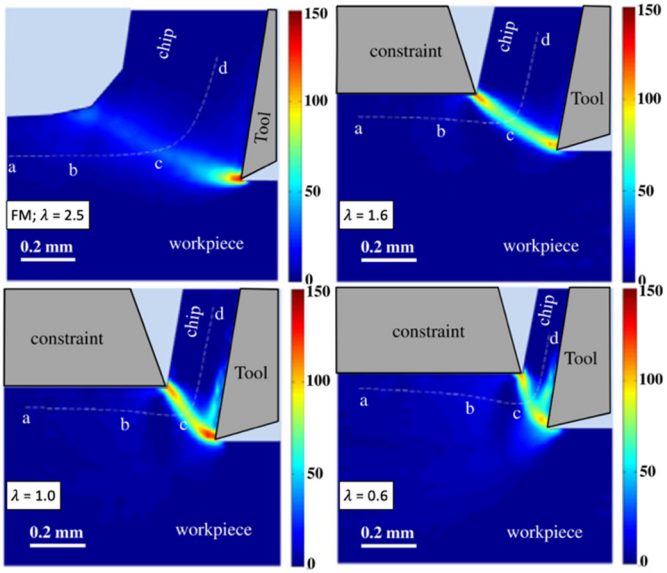

Figure 3.3 Strain rate field in HCE/FM showing localization of deformation, intense straining and deformation path for strip produced by the shear-based processing. $\lambda = 0.6 - 2.5$.

Figure 3.4 is a graphical representation of Eq. 3-1. It shows how the effective strain changes as a function of lambda for three different set rake angles, with important implications for sheet/strip texture and microstructure control. The minimum effective strain always occurs at $\lambda = 1$, and is independent of α. The strip grain size is determined by ε, usually becoming smaller into the ultrafine grained (UFG) range with increasing ε. The lower limit for λ is based on the machine power capability, while the upper limit is usually defined by the workability of the workpiece material.

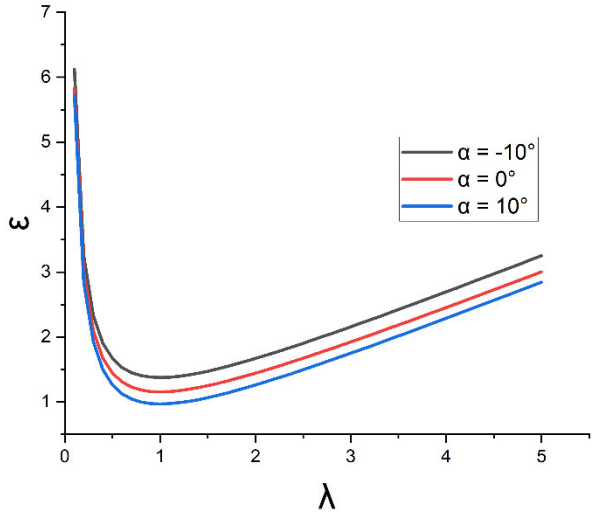

Figure 3.4 Dependence of effective strain (ε) on λ and α.

An important feature of strip production via FM/HCE is the possibility of varying the deformation path by setting different λ or α. Changing the deformation path in machining allows one to control the shearing path during deformation, and, by extension, the crystallographic texture in the strip. This is in contrast to rolling. By enabling shear textures in the strip, the formability of the HCE/FM strip can potentially be improved relative to rolled strip. Thus, FM and HCE make possible production of strip with shear textures, which is not possible with traditional rolling. Likewise control of the strain level via λ or α (i.e., ε) enables strip to be engineered with fine-grained and UFG microstructures. **Figures 3.3 and 3.4** also show how the deformation path changes as a function of λ.

Additionally, during HCE and FM strip formation, there is heat generation in the process zone due to the intense localized plastic deformation (adiabatic deformation-induced heating). The shear plane model allows one to predict the strip temperature in the narrow deformation zone as:

$$T = \frac{(1-\Gamma)U_s}{\rho c} + T_0 \qquad (3\text{-}2)$$

with Γ is the fraction of heat going into the workpiece, U_s as the specific shear energy of chip formation and can be obtained from cutting force, T_0 as the initial workpiece temperature, and ρ and c are the density and heat capacity of the workpiece, respectively. Typically, the increase in temperature in the strip due to the adiabatic heating can be as high as 200 to 600°C. Such adiabatic heating can improve the workability of the material in the process zone, besides influencing strip microstructure by dynamic recovery and recrystallization.

4. Large-Scale Strip Production by Machining-Based Processing: Results

4.1. Prototype machine systems and tooling

Two configurations were used to study large-scale strip production – rotary configuration for strip/sheet/foil widths of up to 50 mm; and a linear planing configuration for strip widths of 50 mm to 150 mm. These two configurations were discussed in the previous Section 3 along with the underlying mechanics. Larger or smaller strip widths can also be produced within each of these systems by use of suitably sized tools and workpieces. These configurations were implemented via two custom-built machine (prototype) systems, designed and supervised by M4 Sciences LLC. The rotary configuration was structured around a 50-HP Okuma lathe, while the linear configuration was built around a 10-HP Hurco machining center. The very large-scale tungsten carbide tooling for these processes was also designed by M4 Sciences LLC, and specifically built for us by Seco Tools (Fagersta, Sweden) at no cost to the project. The tools were both straight WC-Co alloy tools and WC-Co tools coated with abrasion resistant (hard) titanium nitride. The latter tools are distinguished by their well-known golden color. The cutting edge and constraining die/edge widths ranged from 25 to 200 mm, concomitant with the strip width. Both of these are unique first-of-a-kind tools that have never been built before in the machining sector.

Figures 4.1 through 4.5 show various elements of the scaled-up prototype systems for 50 mm and 150 mm wide strip – machine, tooling and cutting tools.

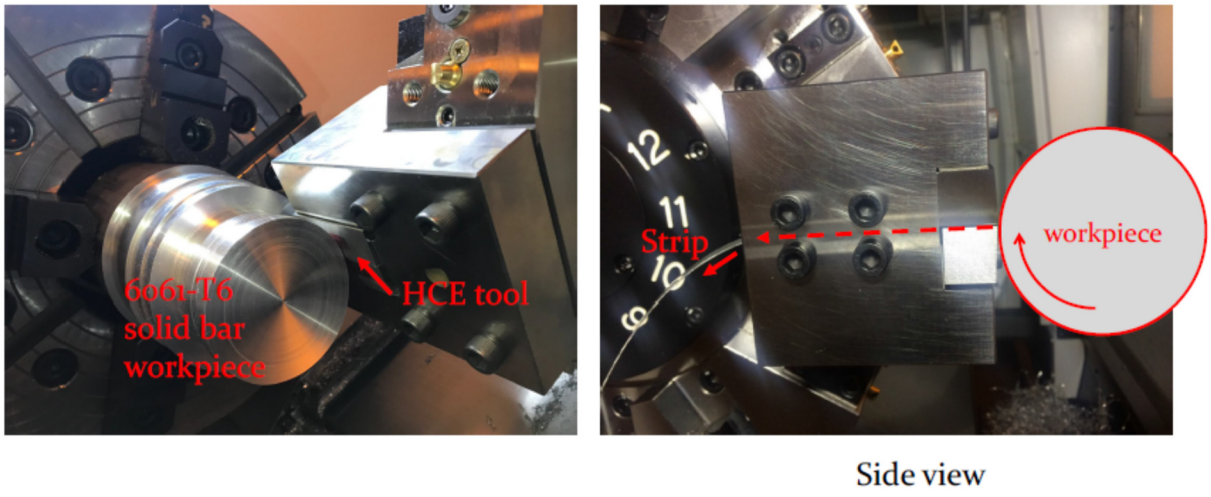

Figure 4.1 Rotary scaled-up prototype system for strip (left) Large HCE tool set-up for producing up to 50 mm wide strip (right) shows how strip emerges from the rear side of the HCE tool via a channel. The system is shown with an Al-6061 alloy workpiece.

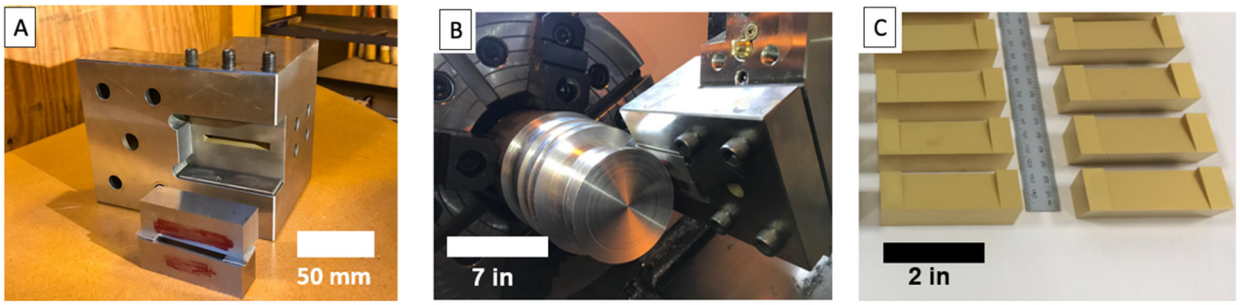

Figure 4.2 FM and HCE setup for production of wide strips (50 mm width). A) Tooling B) Cutting tool engaging the workpiece, B) 50 mm wide tool inserts made of WC-Co with TiN coating.

Figure 4.3 Base Machine for 150 mm wide strip – Linear configuration. The picture on the right is a rendering of the physical process configuration layout within the machine.

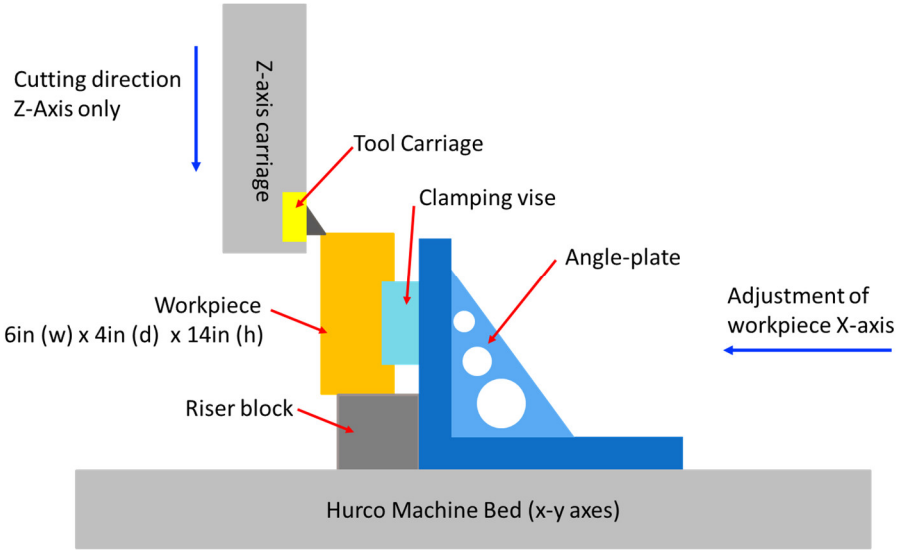

Figure 4.4 Schematic of the machining-based prototype system for large-scale 150-mm wide strip production. This is the configuration within the base machine shown in **Fig. 4.3**.

Figure 4.5 Large-scale tooling for 150 mm wide strip. The tool shown here is a first-generation high-speed steel (HSS) tool.

4.2. Workpiece design

The Fe-4Si-4Cr experimental alloy workpieces were cast and forged to Purdue specifications by Sophisticated Alloys, Inc., Butler, PA. Additional processing was done by Purdue using hot/cold forging facilities at Haynes International. Details of workpiece characteristics and preparation can be found in **Figs. 4.6 through 4.8.** The base workpiece material hardness was ~230 HV

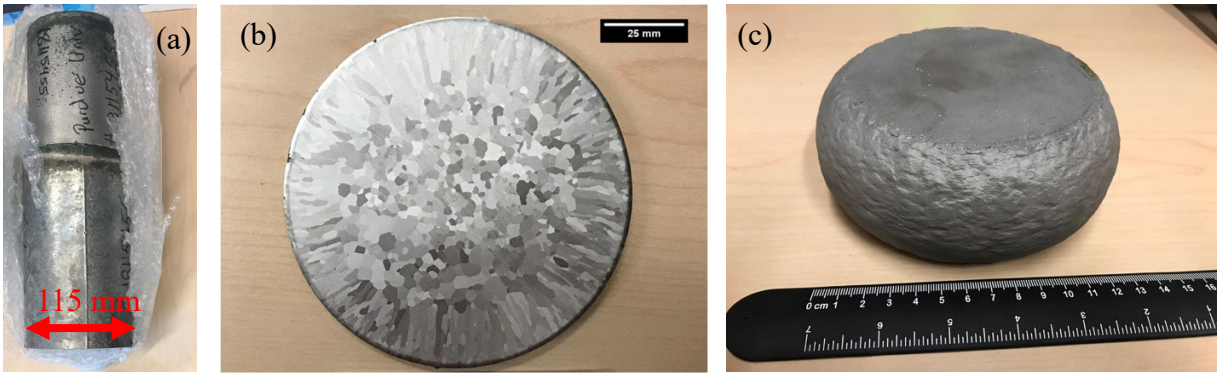

Figure 4.6 Fe-4Si-4Cr alloy workpiece processing for rotary configuration (50 mm wide strip). a) vacuum-cast ingot, 4.5 in diameter, ~50 lb (chemical analysis: 4.02% Si, 3.88% Cr, < 0.01% C, S, O), bottom half cut off for forging. b) As-cast microstructure showing sound, large-grain structure, hardness 230 HV. c) Upset forged (1200ºC) billet for disk-shaped workpiece.

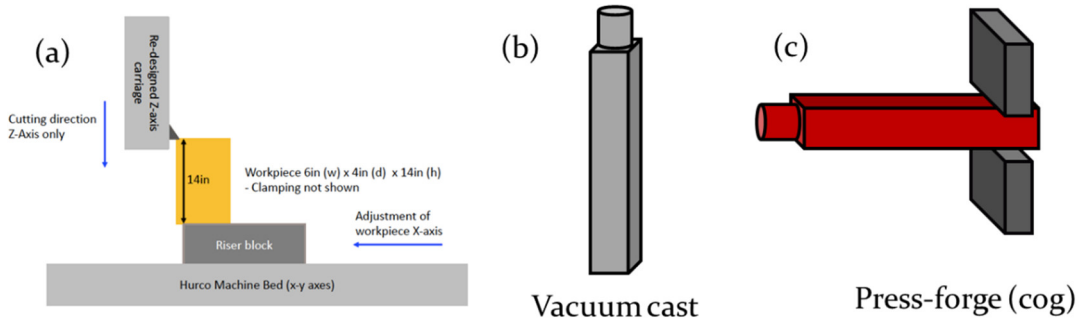

Figure 4.7 Linear configuration workpiece details (150 mm strip). a) HCE process configuration; and b) and c) Process sequence to prepare initial Fe-4Si-4Cr workpiece. Vacuum-cast ingot (~150 lb), press-forged to 4.5 x 6.5 in (see **Fig. 4.8**)

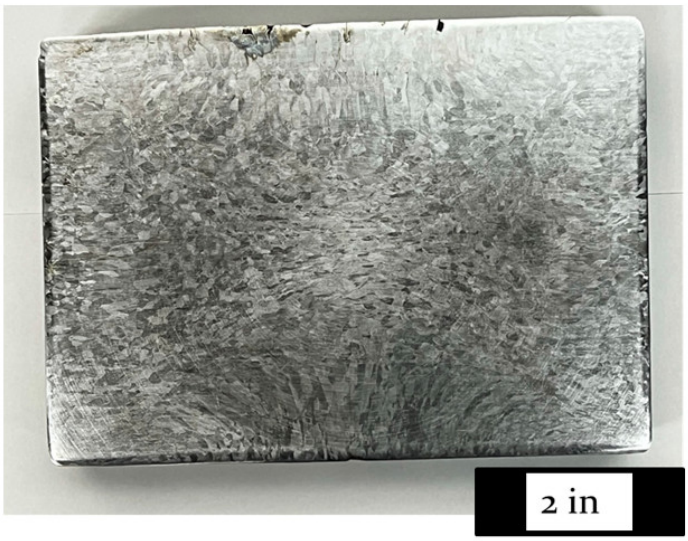

Figure 4.8 Macrostructure of cross-section of Fe-4Si-4Cr alloy workpiece used with the linear configuration.

4.3. Large-scale strip characteristics

Figures 4.9 and 4.10 show typical strips from the experimental Fe-4Si-4Cr alloy and from Al 6061-T6 alloy. The capability of the machining-based processes to produce wide strip with good surface finish is quite clear. Surface roughness measurements on more than 5 strips at various process conditions, using optical profilometry, showed the Sa values for the machining-strips to be typically in the range of 0.35 to 1 μm (**Fig. 11**), very similar that of rolled strip (~ 0.6 μm and above). See also second row in **Fig. 4.22** for typical surface topography pictures.

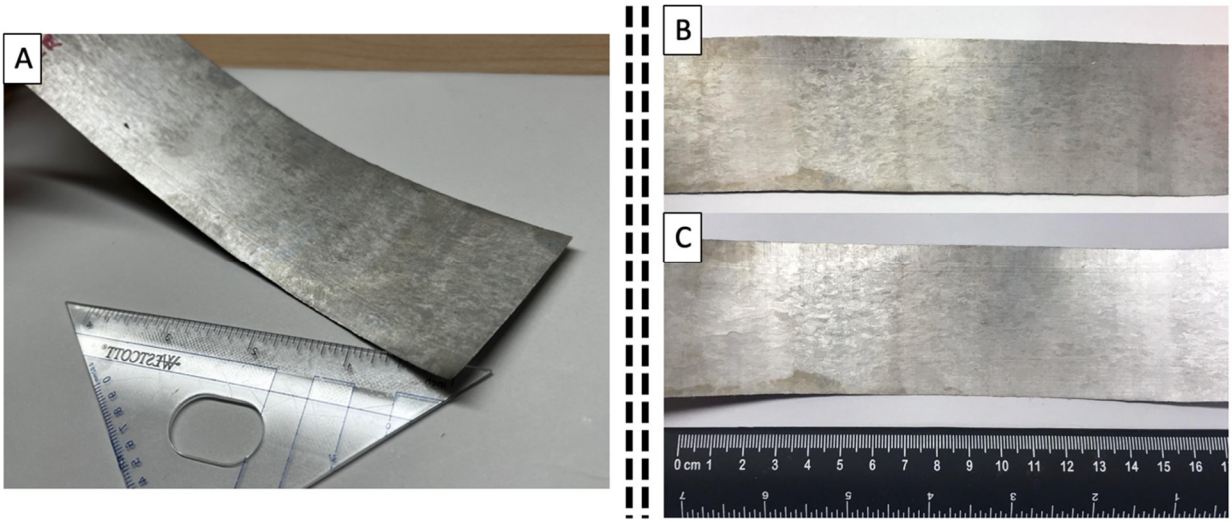

Figure 4.9 50 mm wide continuous Fe-4Si-4Cr strip of thickness ~ 0.35 mm. A) Isometric view, B) top view of the rake face, and C) top view of the constrained face. Process parameters: V_o = 2 m/s, λ = 1.6, α = 20°.

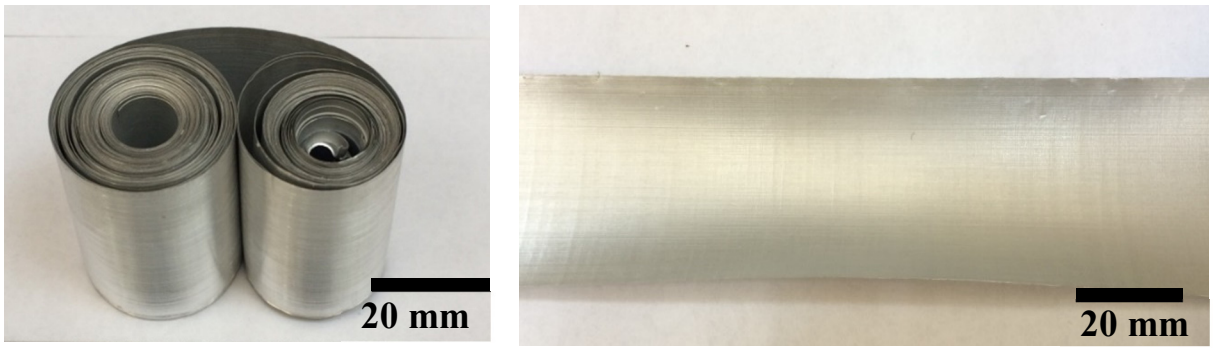

Figure 4.10 Large-scale strip from the Al6061-T6 alloy.

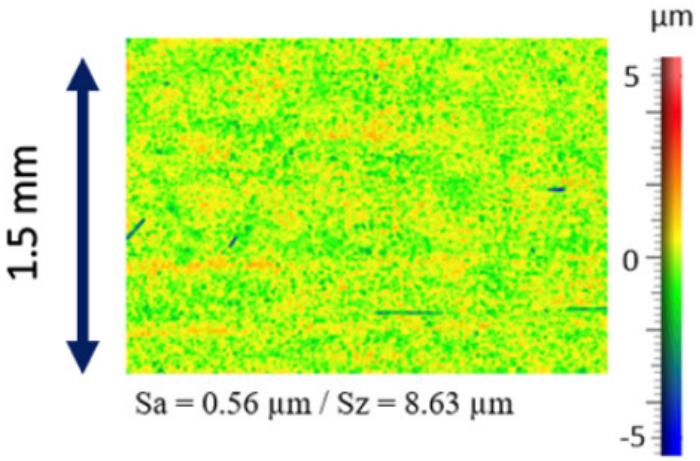

Figure 4.11 Optical profilometry showing sub-micrometer surface roughness (Sa) on the rake face of a 50-mm wide Fe-4Si-4Cr strip.

The through-thickness micro/macro structure for the machining-based strips are shown in **Figs 4.12 and 4.13**. The inclined flow-line microstructure in the bulk of the strip is typical of large-strain deformation, with the flow line inclinations pointing to a crystallographic shear texture (subsequently confirmed by EBSD). The deformation path can also be deduced from the flow lines. Along the top and bottom surfaces of the strip, in a thin near-surface region, the flow line structure is curved – a consequence of friction-induced (secondary) deformation. These strip surfaces are in contact with the cutting and constraining tools. **Figure 13** also shows the effect of strip thickness ratio λ (parameter controlling strain and microstructure) on the flow line (shear texture) pattern and strip product hardness. It may be noted that the strip hardness is about 1.5 X the base material hardness (~ 240 HV). Similar hardness increases have been observed in other alloy strip produced by the HCE and FM+CR, see for example the brass 260 strip with high-quality surface finish shown in **Fig. 14**.

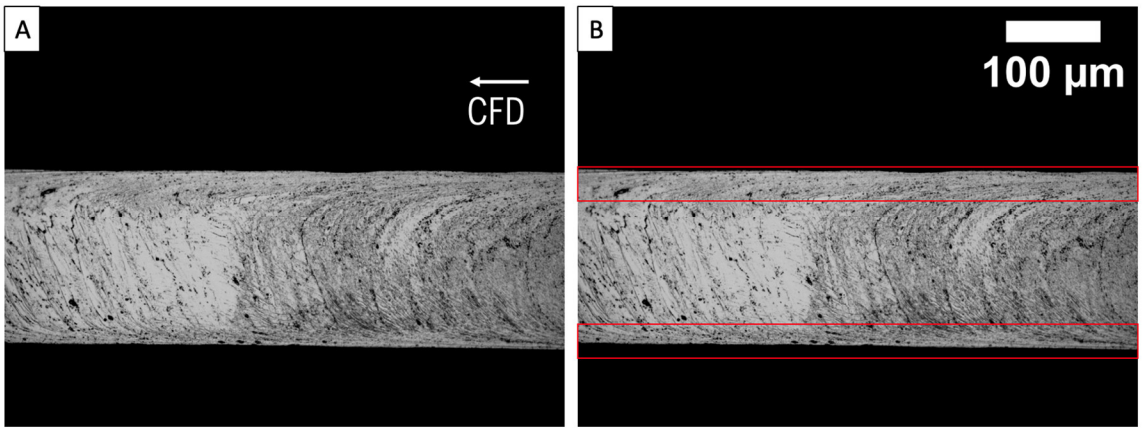

Figure 4.12 (left) Flow-line microstructure of Fe-4Si-4Cr HCE strip. (right) Secondary (friction) deformation zone demarcated by the two red rectangles.

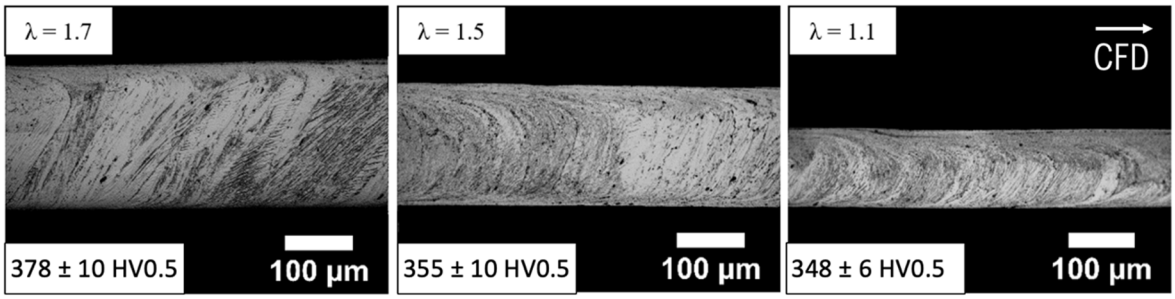

Figure 4.13 Microstructure of strips with three different λ and their respective Vickers hardness.

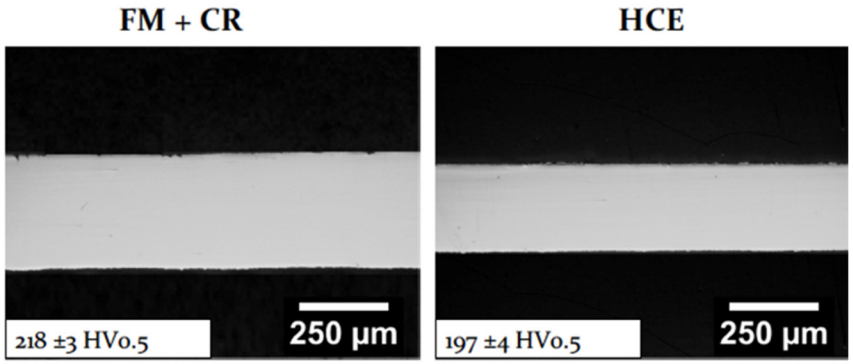

Figure 4.14 Through-thickness cross-section of brass 260 strip (18 mm wide) produced by FM+CR and HCE.

Various annealing treatments can be utilized to optimize strip hardness and ductility analogous to rolled strip. For comparison, the through-thickness microstructure of a rolled conventional electrical steel strip is shown in **Fig. 4.15**. This is a very typical rolling microstructure, wherein the grains are elongated and aligned with the direction of rolling. The alignment is a consequence of the deformation path in rolling. Unlike the machining-based shear deformation processing, the deformation path in rolling cannot be varied over any significant range precluding development of shear textures favorable for formability.

Dynamic recrystallization Another unique feature of HCE related to microstructure control is the possibility of obtaining fine equiaxed grain structures right after cutting, via dynamic recrystallization (**Fig. 4.16**). **Figure 4.16A** shows typical deformed microstructure of HCE strip, while **Fig. 16C** shows a microstructure with coarse equiaxed grains resulting from annealing the HCE strip of **Fig. 4.16A** for 75 minutes at 1100 °C (static recrystallization). The strip in the middle (**Fig 4.16B**) appears to show the usual deformed HCE strained microstructure; but upon closer inspection, this strip is seen to have an equiaxed grain structure with fine grain size of 2-3 µm (see **Fig. 4.16D**). This is a consequence of in situ dynamic recrystallization occurring during the HCE process in this case.

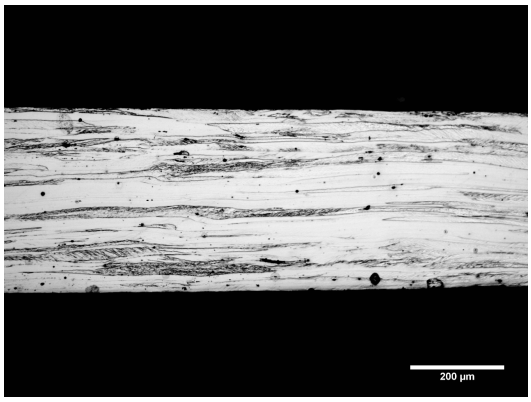

Figure 4.15 Microstructure of rolled electrical steel sheet. The picture shows grains elongated and oriented along the rolling direction.

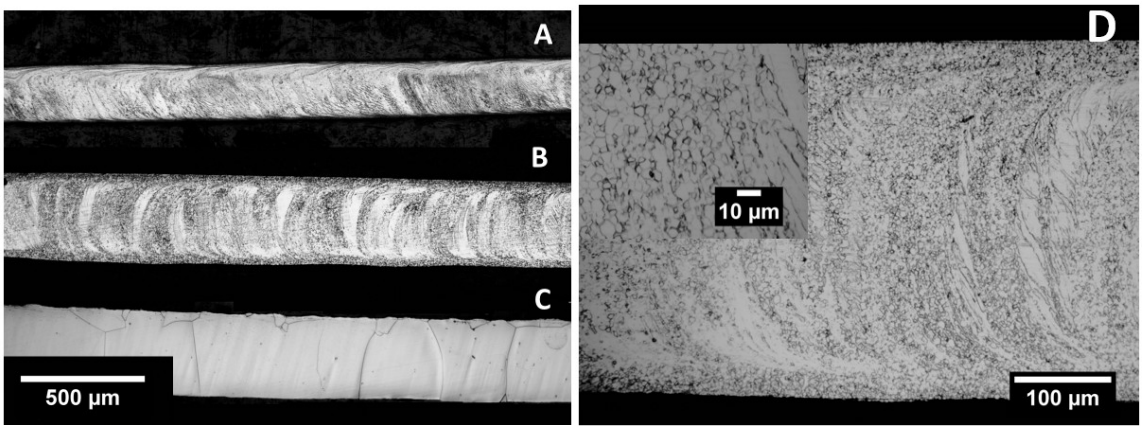

Figure 4.16 Three different HCE strips with different microstructures. A) Highly strained, B) dynamically recrystallized, C) statically recrystallized, and D) zoom-in of the dynamically recrystallized strip. CFD to the left of the micrographs.

To understand this dynamic recrystallization, we may recall that large-strain and high strain rate deformation processes like machining are characterized by a narrow shear deformation zone with significant adiabatic-deformation heating therein. The sample shown in **Fig. 4.16B** was produced at a speed of 8 m/s, as compared to the strip in **Fig. 4.16A** which was produced at 3 m/s. The transition from a highly deformed microstructure to fine equiaxed grains is due to the large adiabatic temperature rise in the deformation zone due at the higher speed condition **(Fig. 4.16B)** - a classic case of dynamic recrystallization. Dynamic recrystallization is a metallurgical phenomenon that can be explained as a process of nucleation and growth of new grains (by dislocation substructure rearrangement) during the deformation process itself. The capability of the HCE process to effect dynamic recrystallization at select process conditions and create fine-grained equiaxed microstructures is another positive benefit of the machining-based processing for strip production.

Annealing and texture development Annealing studies were conducted to establish the static recrystallization kinetics of the Fe-4Si-4Cr strips produced by HCE and by rolling. Detailed metallographic analysis using both optical and orientation imaging microscopy (EBSD) enabled the development of maps defining the process stages (recovery, recrystallization and grain growth) in temperature-time space. Although the annealing kinetics of the HCE and rolled strips were quite similar, their resulting microstructures showed significant differences. Microstructure and texture development was studied further using EBSD. **Figure 4.17** shows EBSD pole figures from the HCE strip and the evolution of texture through annealing. The pole figures directly show the <111> and {110} partial fiber textures with inclination to the strip normal corresponding closely to the shear flow lines (e.g., **Fig. 4.13**) through the thickness of the strips. Furthermore, the shear texture, which can be controlled by the HCE parameters, is retained through annealing to the fully recrystallized (soft) condition needed for application. In contrast, the rolled strip exhibits heavily banded deformation structure and inhomogeneous grain structure evolution in annealing (see **Fig. 4.22**, attribute 5).

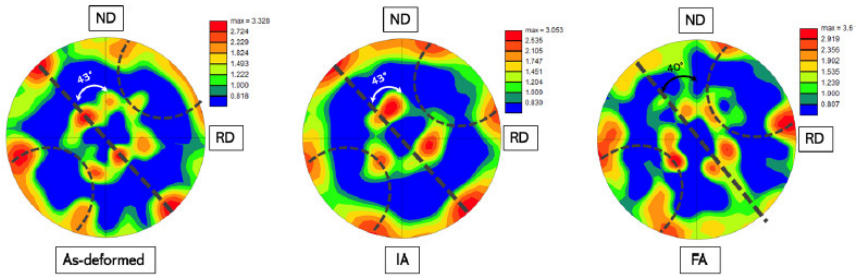

Figure 4.17 Texture evolution in Fe-4Si-4Cr HCE strip based on (110) pole figures measured by EBSD. A strong shear texture in the as-deformed strip (left), with <111>-fiber component inclined the strip normal direction, is maintained through intermediate (middle) and full (right) recrystallization annealing.

Hardness and formability **Figure 4.18** shows that the hardness is quite uniform across the width of the HCE strip, as are strip thickness and surface roughness. **Figure 4.19** shows the results of comparative formability testing – HCE experimental alloy strip against conventional rolled M-19

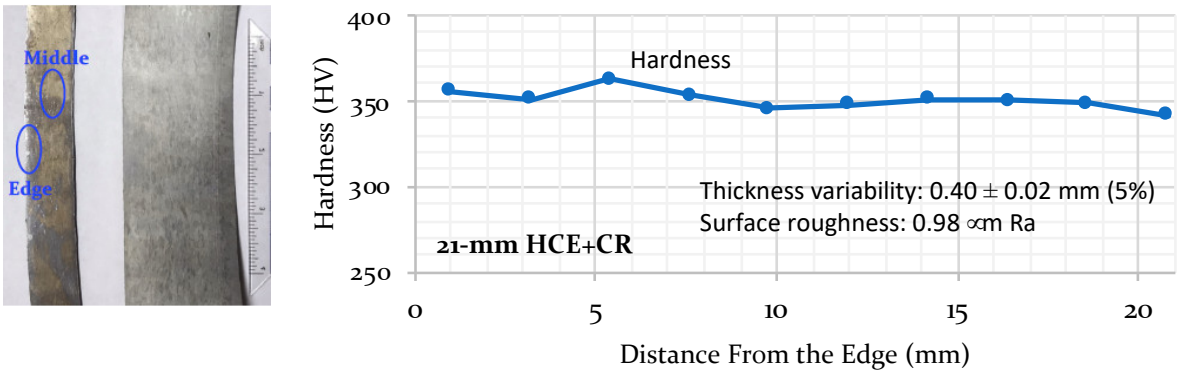

Figure 4.18 HCE strip of up to 48-mm wide characterized for uniformity. Graph shows edge-to-edge hardness variability on a 21-mm HCE+CR strip, along with thickness variability and surface roughness.

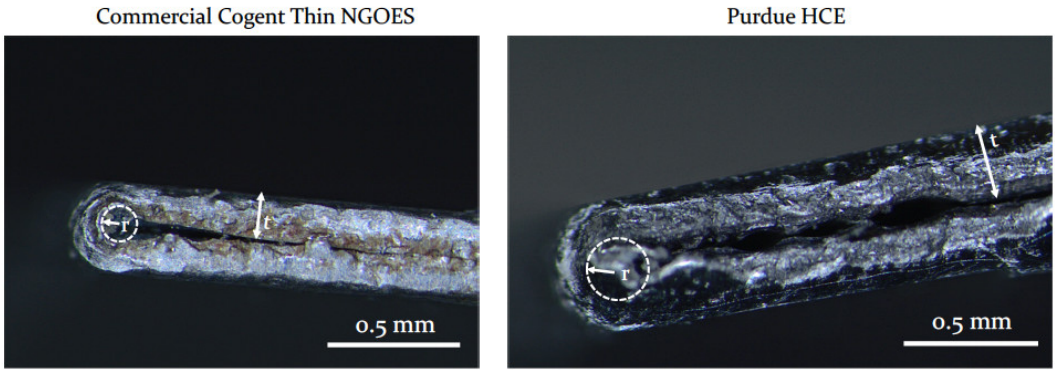

Figure 4.19 Formability evaluation using bend testing. Both the commercial rolled + annealed (M-19 steel, 3% Si) strip and the HCE experimental alloy strip are seen to withstand 180° bending (complete folding over) without cracking, indicative of high formability in the strips.

steel sheet (3% Si). These results are from 180-degree bend testing. The HCE strip is seen to match the bend formability of the rolled M19 sheet. A detailed characterization of strip is presented in section 7 in the context of punching characteristics of strip.

4.4 Very large scale strip production

The project has culminated in recent demonstration of discrete strip of 150 mm width X 0.4 mm thickness from 316 stainless steel, and 100 mm width from commercially pure copper, using the very large-scale WC tooling with the linear machining-based platform. Some of this strip production has benefited from addition of an innovative "mechanochemical component" to the machining process. This mechanochemical component involves coating of the large workpiece (surface) with thin organic ink film, prior to the cutting. The ink-film stabilizes the material deformation during the machining processing, enabling high-quality strip to be produced even from large workpiece ingot with highly variable microstructure. Examples of the very large-scale stainless steel and copper strips, with good surface finish, are shown in **Figs 4.20 and 4.21**. Similar 150 mm wide strip has also been produced from the experimental Fe-4Si-4Cr alloy but the surface

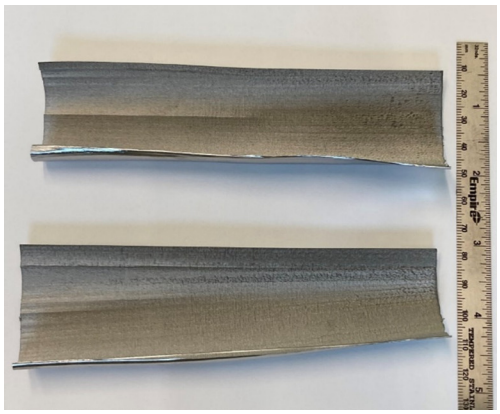

Figure 4.20 150-mm wide 316SS strip by the machining-based processing.

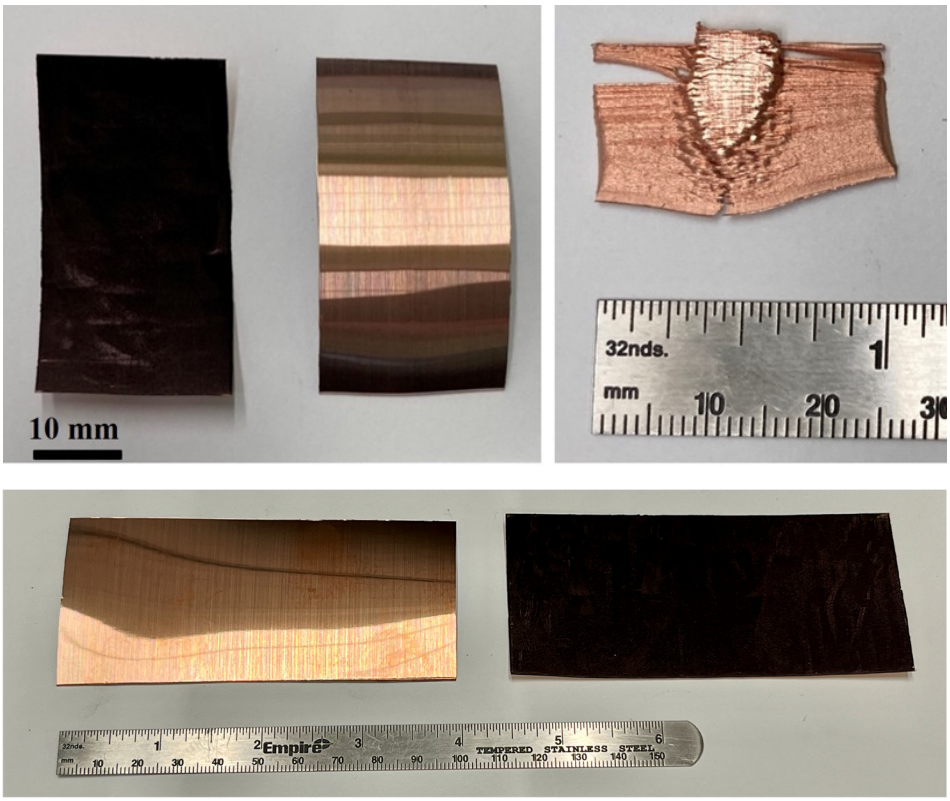

Figure 4.21 (top) 25-mm wide copper strips produced by the machining processing – continuous strip of high quality enabled by use of organic media (ink) adsorbates (mechanochemical effect), and strip with fractures (right) due to workpiece microstructure heterogeneity (without adsorbate). Note the remarkable transformation from a fractured strip to continuous strip enabled by the mechanochemical effect. (bottom) 100-mm wide high-quality copper strip produced using the mechanochemical effect.

quality is not yet up to the mark. This has been traced to the very poor macro/micro structure of the initial workpiece. Efforts are ongoing now to improve the initial workpiece structure for achieving improved strip surface quality.

A comparative summary of attributes of Fe-Si alloy strip by the machining-based processing and conventional multistage rolling is given below (**Fig. 4.22**).

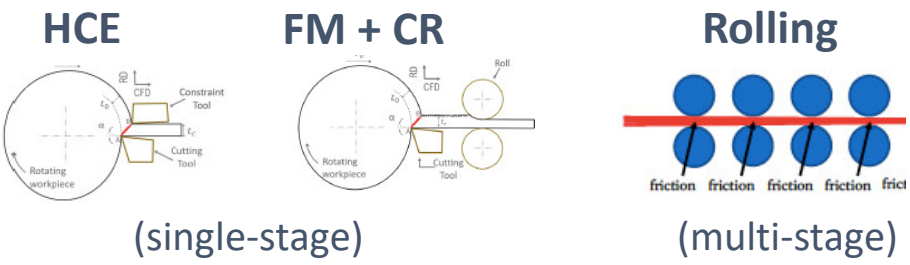

(single-stage) (multi-stage)

Attributes

Remarks

1. Surface finish, Sa (μm) 0.4/1.0 (rake/constraint) ~ 0.6*

*Typical cold-rolled surface finish

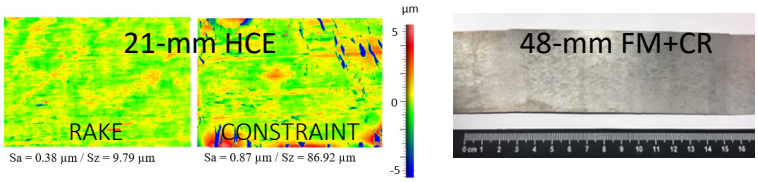

2. Microstructure

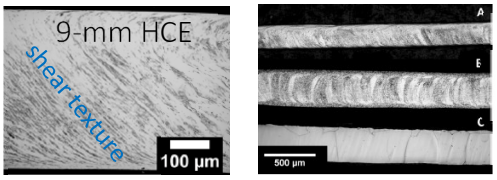

Strain-hardened
Dynamically recrystallized
Annealed

Wide range of control in HCE, including unique shear textures

3. Hardness HV 378 (as-HCE) to 230 (full anneal)

395 for Fe-6.5 Si; not cold-rollable

4. Force/Energy HCE energy is less than 25% rolling energy

Specific energy analysis

5. Recrystallization

Grain size control, from 3 μm to strip thickness

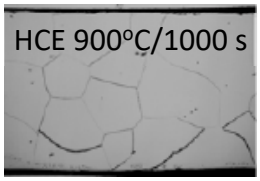

Banding

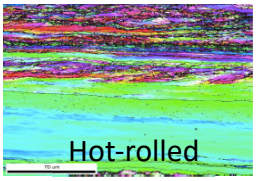

Recrystallization kinetics fully characterized

6. Formability (V-bend)

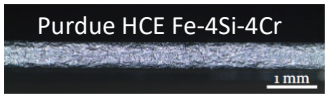

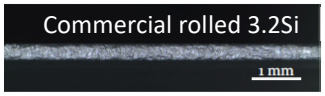

HCE strip comparable to commercial rolled 3.2 Si alloy

Figure 4.22 Comparison of strip quality and process attributes for the shear-based (machining) processes and conventional rolling.

5. Magnetic Properties

In this section we examine the magnetic properties of the Fe-4Si-4Cr experimental alloy, compare these properties with those of a baseline Fe-3.2%Si alloy, and show that the properties of the experimental alloy are consistent with DOE program requirements.

5.1 Background

One of the specific objectives of the project is to produce Fe-Si-Cr sheet with core loss lower than commercial benchmark Fe-3.2Si wt% (M19 electrical steel or equivalent). For this purpose, a new electrical steel alloy (Fe-4Si-4Cr) has been developed with better magnetic performance (see ensuing) than ~Fe-3.2Si wt% and good workability. Fe-3.2Si wt% is selected as a control alloy because this alloy has the highest Si content among electrical steels in large-scale industrial use. **Table 5-1** contains detailed information on the magnetic properties of commercial M-19. The table also gives the magnetic properties data for an alloy called DI-MAX HF-10X, that is very similar to the M19 steel. This DI-MAX HF-10X alloy is used as the control sample for property comparisons.

Table 5-1 Properties of commercial electrical steels used as control samples, DI-MAX HF-10X and M19[1] (both sourced from AK Steel).

Property	**DI-MAX HF-10X (0.25 mm) AK Steel**	**M19 (0.35 mm) AK Steel**
Resistivity ($\mu\Omega \cdot cm$)	60	55
Core loss @ 1.5 T/60 Hz (W/kg)	2.46	3.48
Core loss @ 1.5 T/400 Hz (W/kg)	29.6	42
Saturation Induction (T)	1.97	1.99
Hardness (Vickers)	193	180
Density (g/cm^3)	7.6	7.65
Yield Strength (MPa)	440	421
Composition (wt%)		3.3%(Si + Al)
Grain Size (μm)	60	170

[1]Bertotti et al. and AK Steel data

Magnetic properties characterization was performed at Magnet-Physics, Inc in Indianapolis, following ASTM A773/A773M-21 for DC testing and ASTM A927/A927M-18 for AC testing. To evaluate the magnetic properties of the Fe-4Si-4Cr experimental alloy, both rolled and machining-based strip samples of this alloy were used. In addition to the experimental samples, a commercial material was also tested. The technique used to evaluate the magnetic properties is called the toroidal test (more details of the test are given in the Experimental sub-section of this chapter). The technique uses ring samples of electrical steel sheet that are stacked up to form a small magnetic core**. Figure 5.1** shows a schematic of the magnetic core and the ring samples used in the present experiments.

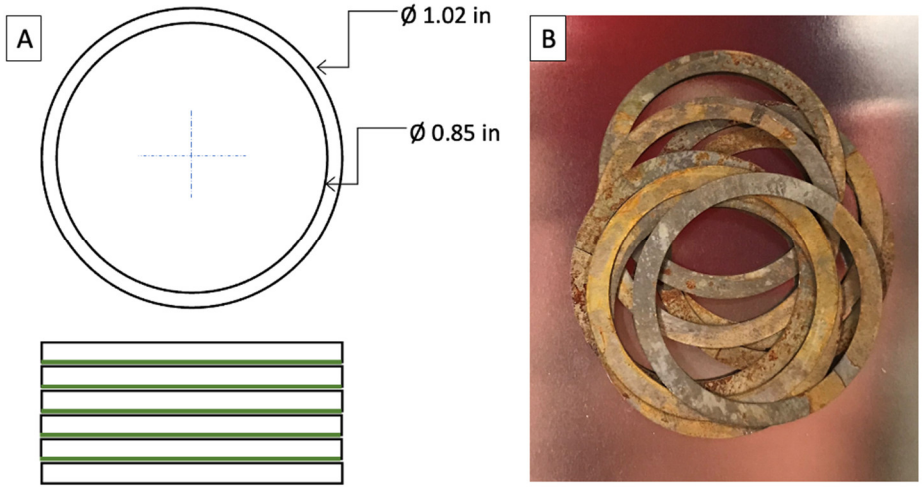

Figure 5.1 a) Schematic of the toroidal testing setup used in this project, and b) Fe-4Si-4Cr rings produced for magnetic testing via EDM.

There are some restrictions related to the geometry of the rings used for the toroidal test, for example, the ratio of the outside to inner diameter. However, there is no minimum or maximum ring size defined in the ASTM standard. In practice, a very small ring size is avoided because of the low intensity of magnetic flux close to the center of the toroid. In this project, the minimum outside ring diameter used was ~ 25 mm, which was cut out of the 50 mm FM+CR strips of Fe-4Si-4Cr. The ring sample thickness was ~205 µm, which is somewhat smaller than the minimum thickness of commercially available M-19 samples (0.36 mm). Bertotti's model encapsulated in the Eq. 5-1 below can be used to calibrate for the effect of the sheet thickness on the core losses. This model is widely used to study the core losses of electrical steels.

$$P_s = \underbrace{\{C_0 B_m^{\alpha} f\}}_{P_h} + \underbrace{\left\{\frac{\pi^2 d^2 B_m^2}{6\rho\gamma}\right\}}_{P_e} + \underbrace{\left\{C_1 B_m^{3/2} f^{3/2}\right\}}_{P_a} \tag{5-1}$$

where B_m = Max flux Density, f = frequency, d = sheet thickness, ρ = electrical resistivity, γ = material density, and α, C_0 & C_1 are constants characteristic of material obtained via curve fitting. Knowing three experimental points of the equation is enough to determine unknown constants.

Basically, the higher the sample thickness, the higher the eddy current losses. Hence for comparison, the rolled and commercial control samples must have sheet thickness close to the FM+CR sample. The commercial alloy called DI-MAX HF-10x, with sheet thickness close to 205

μm and similar to the M19 commercial alloy, was used as the baseline alloy for properties' benchmarking. In this section, the magnetic properties of the Fe-4Si-4Cr experimental alloy are measured and compared with the control sample of the commercial alloy DI-MAX HF-10x.

5.2 Experimental methods

The magnetic property characterization was performed at Magnet-Physics Inc in Indianapolis. To evaluate the magnetic properties of the Fe-4Si-4Cr experimental alloy, three conditions were identified – machining-based Fe-4Si-4Cr, rolled Fe-4Si-4Cr, and commercial alloy (DI-MAX HF-10x). The ingot for the rolled sample (as well as the FM+R) was manufactured by Sophisticated Alloys Inc. The samples were hot rolled from 10 mm to 2 mm. After hot rolling, the plates were cold rolled to 400 μm with an intermediate annealing of 5 minutes at 800 °C. To obtain a final thickness of ~200 μm, the samples were "sandwiched" between laminations of the same material and further cold rolled. The commercial alloy DI-MAX HF-10x sheet was obtained from AK Steel in the fully processed condition.

The rings for the magnetic toroid testing (**Fig. 5.1**) were cut out from each material using electro-discharge machining (EDM). After cutting, the rings were heat treated at 800 °C for 1 h in a convection furnace. A thin layer Rust-Oleum-brand Crystal Clear Enamel spray was then applied to one side of each lamination ring. This coating in addition to the thin oxidation (heat treatment) layer helped electrically isolate the different laminations of the stack.

The mass of the test specimens was obtained to 0.001 g accuracy. The ring inner and outside diameter were measured using a caliper with 0.01 mm resolution. The material density was obtained using Archimedes principle. These data were used to calculate the packing factor and the cross-sectional area of the actual testing material.

The DC or quasi-static B-H loop was measured. The AC core loss curves was tested at 60 Hz and 400 Hz, with magnetization levels from near zero up to the flux density level where the form factor of the flux waveform was approximately 1.14. The DC testing was performed using a Magnet-Physik Model Remagraph C-500 Soft Magnetic Test System in accordance with ASTM A773/A773M-21 Standard Test Method and IEC 60404-4. Typical measurement uncertainty in the ring measurements was approx. ± 1% for B and ± 1% for H. The AC testing was performed using a Magnet-Physik Model Remacomp C-1200 test system which corresponds to ASTM A927/A927M-18 Standard Test Method for Alternating-Current Magnetic Properties of Toroidal Core Specimens Using the Voltmeter-Ammeter-Wattmeter Method, and IEC 60404-6 (digital method).

5.3 Results and analysis

The resistivity measured for Fe-4Si-4Cr was **85 ± 3 μΩ·cm.** Strictly speaking, electrical resistivity is an electrical property of a material rather than a magnetic property. Nevertheless, it is important from a magnetism perspective, since the electrical resistivity significantly impacts the eddy current losses - the most important core loss at high frequencies. The electrical resistivity target was ≥80 μΩ·cm based on the value of Fe-6.5Si wt%. The Fe-4Si-4Cr alloy showed a slightly higher resistivity than the targeted value.

Figure 5.2 shows the microstructure of a fully-processed commercial electrical steel (DI-MAX HF-10X) with a thickness of 0.25 mm. The average grain size in the commercial alloy is 60 μm, which is about ¼ of the strip thickness. This grain size-thickness relationship agrees with data seen in the literature. Grain boundaries are known to be deleterious to motion of magnetic domain walls; thus, the bigger the grain size, the better the magnetic properties. However, having grains of a size

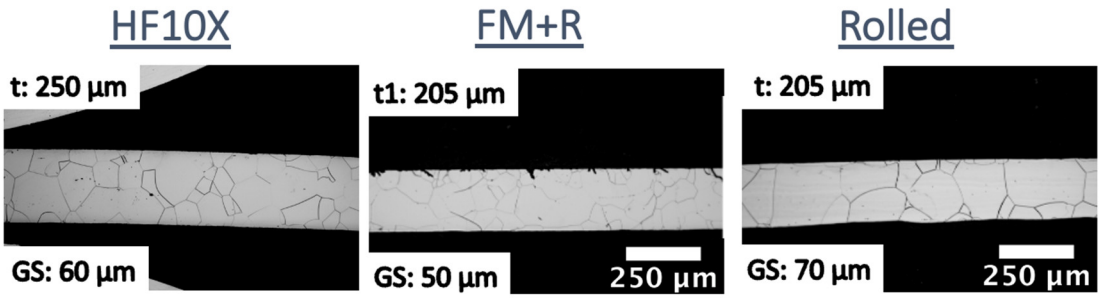

Figure 5.2 Side-view (through thickness) microstructure of samples prepared for magnetic testing of commercial alloy (DI-MAX HF-10X), experimental alloy in (FM+CR) and rolled conditions.

equal to the strip thickness is detrimental to magnetic properties as well. There is a reason why the ideal grain size should be a fraction of the total strip thickness, and it is related to the anisotropy of α-iron. If one has a material with grains as big as the strip thickness, there is a possibility that some of those grains will have the hard direction of magnetization aligned to the rolling direction (RD). A smaller grain size reduces the likelihood of this happening. The microstructure targeted for the machining-based and rolled samples is also shown in **Fig. 5.2**. The average grain size for the commercial material is 60 µm, for the FM+CR sample is 50 µm, and 70 µm for the rolled sample, all comparable to one another.

The microstructure of the actual samples used for the magnetic toroid testing was evaluated via EBSD **(Fig. 5.3).** The HF-10X and the rolled sample effectively resemble the microstructures shown in **Fig. 5.2**. In contrast, this machining-based sample has a coarser microstructure. This coarser grain size is somewhat detrimental to the magnetic performance of the FM+CR sample.

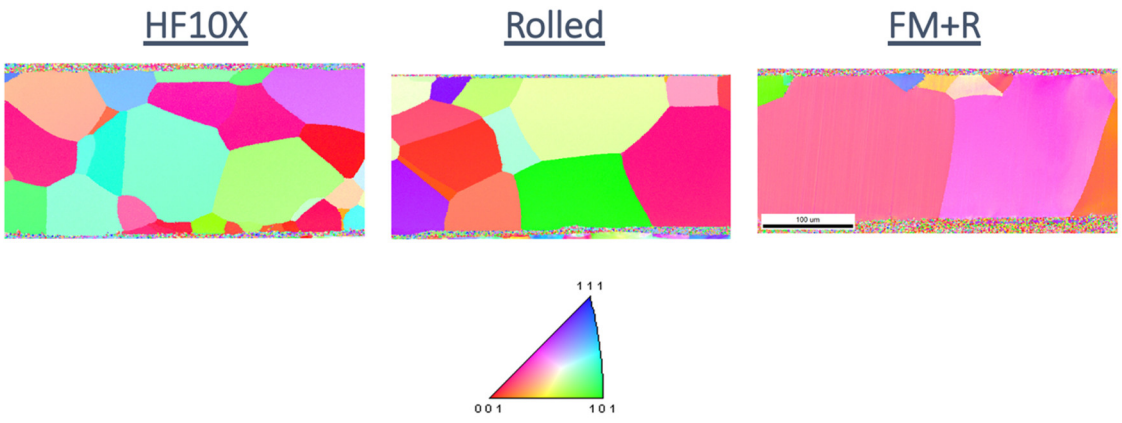

Figure 5.3 Microstructure of the three samples – DI-MAX HF-10X, FM+CR, and rolled. EBSD with the crystallographic direction parallel to RD.

The magnetic properties that characterize soft magnetic materials are high magnetic permeability and flux saturation; and low coercivity, core loss, and magnetostriction. DC testing results are shown in **Fig. 5.4**. The DC loops are useful to evaluate the magnetic permeability, coercivity, and flux saturation. Due to the non-linearity of the magnetic permeability, there are many ways to report it. We report the magnetic permeability using B values and corresponding H values.

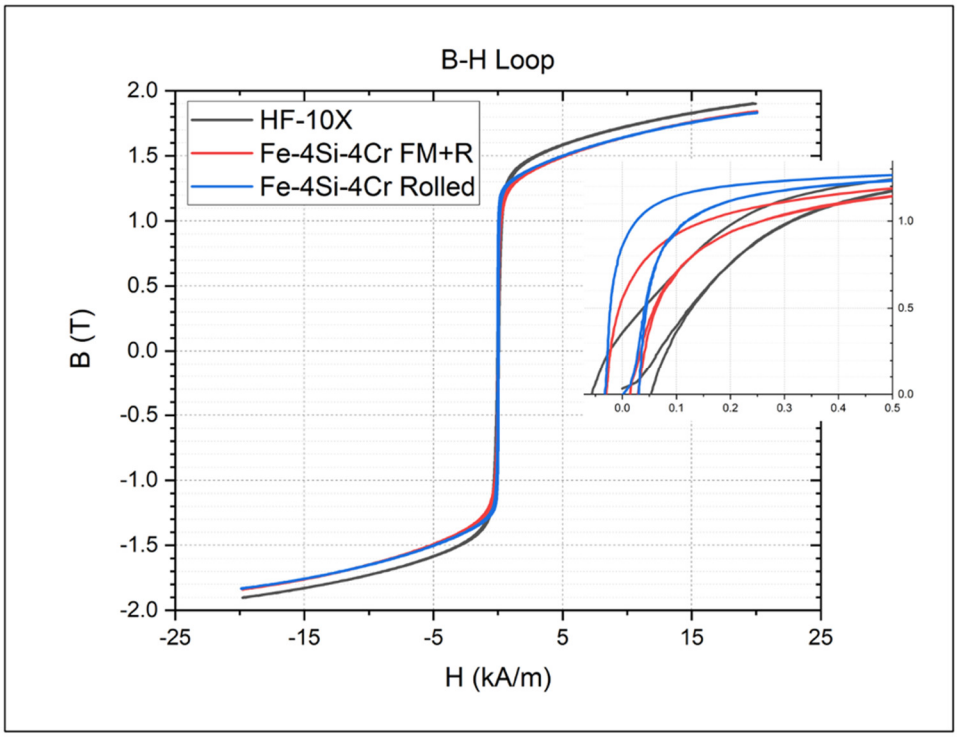

Figure 5.4 DC testing results for the three sample conditions. The figure also shows a zoom-in of the first quadrant that illustrates some of the properties in more detail.

The measured B5 (B [T] at H=500 A/m) was equal to 1.21, 1.17, and 1.25 T for the commercial alloy, the FM+CR, and the rolled sample, respectively. Also, B20 (B [T] at H=2000 A/m) was equal to 1.44, 1.35, and 1.37 T for the commercial alloy, the FM+CR, and the rolled sample, respectively. These results are summarized in **Table 5-2** for clarity. The permeabilities for the three samples at B5 and B20 are similar. The sample with the lowest magnetic permeability at the two conditions is the FM+CR sample. The commercial and the rolled sample switch places at B5 and B20.

The B_{max} for the commercial alloy, the FM+CR, and the rolled sample are 1.9, 1.84, and 1.83T, respectively. These values are within the range of conventional electrical steel B_{max}. The parameter determining the magnetic flux saturation in electrical steel is the Fe at% in the alloy. Both samples of the experimental alloy have the same Fe at% (Fe-4Si-4Cr wt% = Fe-7.6Si-4.1Cr at%). The commercial Fe-3.2Si wt% (Fe-6.7Si at%) alloy has a somewhat higher Fe at% than the experimental alloy.

The magnetic core loss for the experimental alloy in the FM+CR and rolled conditions, and the DI-MAX HF-10X alloy, are shown in **Fig. 5.5**. The experimental alloy samples have the lowest

core loss over the entire range of B(T) at the two frequencies. The rolled experimental alloy sample has the lowest core loss, but the difference between the FM+R and the rolled sample is slight (~5%) and within the experimental uncertainty. This small difference between the FM+CR and rolled experimental alloy samples is likely a consequence of the somewhat larger surface roughness on the FM+CR samples, see also **Fig. 5.2**. The additional small-scale roughness on the FM+CR sample can perturb the magnetic flux, and, consequently, slightly increase the core loss.

The core loss reduction of the Fe-4Si-4Cr samples compared to the control DI-MAX HF-10X sample is ~28% at 60 Hz and ~35% at 400 Hz. The core loss reduction difference at the two frequencies is related to the higher electrical resistivity of the experimental alloy. The core-loss reduction is also greater at the higher frequency. The magnetic property data from the experimental alloy samples and the control commercial alloy sample are summarized in **Table 5-2**.

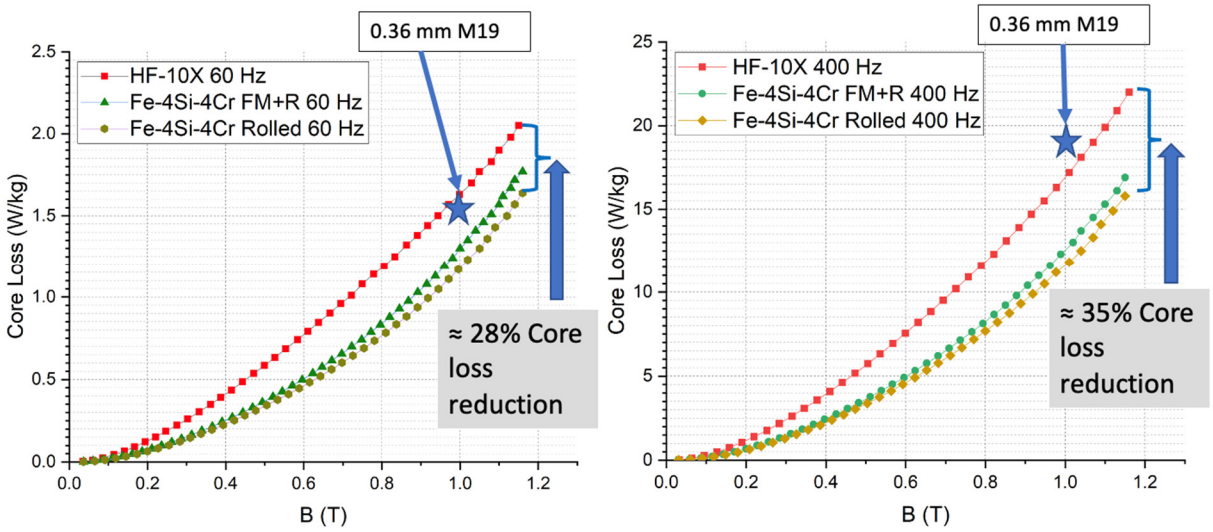

Figure 5.5 Core loss as a function of the flux density for the DI-MAX HF-10X, FM+C, and rolled samples at 60 and 400 Hz. The M19 data (0.36 mm) is also reported as a point in both the figures and closely tracks the control HF-10X data.

In summary, the magnetic characterization shows that the Fe-4Si-4Cr experimental alloy has better magnetic performance than the baseline high-silicon commercial electrical steel alloys. The benefits of the magnetic performance of Fe-4Si-4Cr are even more significant at the higher frequencies. Based on the calculations of the DOE, a reduction of 37% in core losses of electrical motors would save approximately 0.44% of all the electrical energy consumed in the US. Our data shows that the Fe-4Si-4Cr core loss is very close to the 37% core loss reduction objective of the DOE.

The benefits of the magnetic performance of Fe-4Si-4Cr are even more significant at the higher frequencies. Based on the calculations of the DOE (2017) a reduction of 37% in core losses of electrical motors would save approximately 0.44% of all the electrical energy consumed in the US. This chapter shows that the Fe-4Si-4Cr is close to the 37% core loss reduction claimed by the DOE.

Table 5-2 Summary of magnetic properties – commercial control DI-MAX HF-10X alloy and Fe-4Si-4Cr experimental alloy (FM+CR and rolled conditions).

Parameters	HF-10X	FM+CR	Rolled
$\boldsymbol{\rho}$ **[μΩ · cm]**	60	85	85
$\boldsymbol{B_{max}}$ **[T]**	1.9	1.84	1.83
$\boldsymbol{B5}$ **[T]**	1.21	1.17	1.25
$\boldsymbol{B20}$ **[T]**	1.44	1.35	1.37
$\boldsymbol{H_{CB}}$ **[A/m]**	54.9	29.3	31.3
Core Loss [W/kg] @1T & 60 Hz	1.7	1.3	1.2
Core Loss [W/kg] @1T & 400 Hz	17.2	13	11.8

6. Energy Analysis of Rolling Processes

In this section, we present an energy analysis for multistage rolling process used to produce sheet from billet/ingot. We present the energy analysis model and apply it to several available industry rolling schedules for Al and stainless steel alloy sheet. We show that the rolling process is quite energy intensive compared to the single-step FM and HCE process for strip.

6.1. Introduction and rationale

The rolling process is widely used in industry to make sheet and foil. Usually the thickness reductions are large, with many stages of incremental deformation (1000/500 mm initial ingot size to 1 to 2 mm final sheet thickness) between the initial ingot stage and the final sheet/strip product. A typical rolling schedule is multistage comprised of hot and cold rolling steps (**Fig. 6.1**) – hot for the early stages involving large thickness reductions, which involves heating of large workpieces; followed by later cold rolling stages for obtaining good sheet metallurgical properties and surface finish. The hot and rolling stages are often interspersed with intermediate cleaning and annealing treatments – for example, between the cold rolling stages there may be annealing steps to recover ductility; and in the hot rolling case, cleaning of the surface by pickling etc. to remove scale.

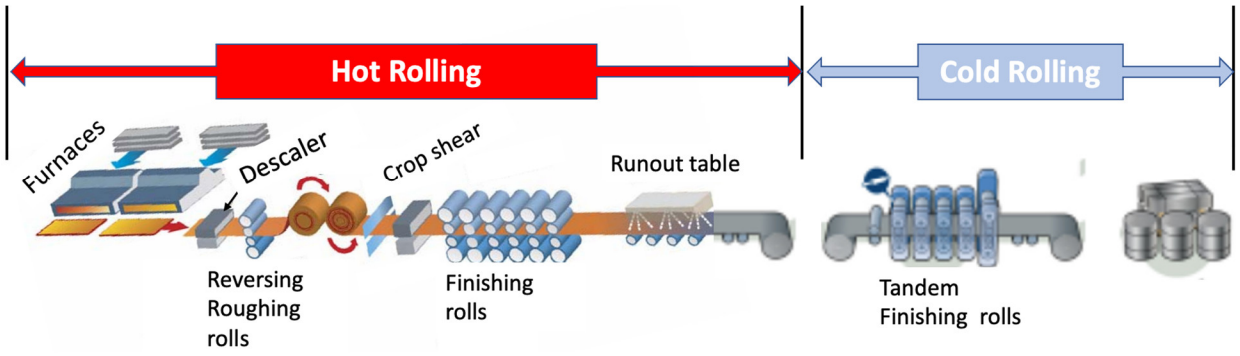

Figure 6.1 Typical multistage Rolling production line

Because of its multistage nature involving workpiece heating, and hot and cold deformation steps, the energy consumption in rolling has been suggested to be large. Yet the estimates of this energy are few and far between – the most widely cited reports for the large energy dissipation are the pioneering ones prepared by Fruehan et al.[1] and Sakamoto et al.[2] The Fruehan report essentially calculated the rolling energy as that primarily due to the heating of the workpiece prior to the hot rolling stage (mass x specific heat x temperature). The deformation energy contribution was estimated as being small, based on a primitive model of homogeneous deformation and zero friction, not particularly reasonable assumptions for rolling. The Fruehan report has often been quoted by the DOE to highlight the energy intensive nature of rolling processes in the steel and Al sectors.

[1]Theoretical minimum energies to produce steel for selected conditions; A Report for the DOE, OIT (2000).
[2]Estimation of energy consumption for each process in the Japanese steel industry, Energy Conser. Mgmt.(1999).

The Japanese analysis was based on fuel and electricity inputs into a "control volume system" – a systems calculation approach. This calculation showed the rolling process energy to be the second largest, exceeded only by that for blast furnace operations, in the steels sector. Because this calculation used a control-volume systems approach, it is not particularly useful for identifying which steps in the rolling schedule are the most energy intensive and what can be done to reduce the energy in these energy-intensive steps.

In the present analysis, we address these key limitations in the prior work, building on well-established mechanics of the rolling process. The specific limitations addressed are neglect of a) the role of friction in the deformation processing by rolling; b) the friction hill contribution to the rolling pressure which becomes very large in the latter stages of the rolling process; c) strain rate and temperature effects on material yield stress and process energy; d) the inhomogeneous deformation (primary) contribution to energy in the hot working stages. The modeling and analysis presented here incorporates these aforementioned important factors, providing a framework also for studying process parameter effects on rolling energy. We apply the modeling to various multistage rolling schedules with Al alloys and stainless steels and estimate the specific energy for sheet production – including both the workpiece heating and deformation processing energy components. We show that the deformation energy contribution to the overall specific energy is

significant (as much as a 1/3rd of the overall energy). The specific energy for production of strip by the single-step machining-based FM and HCE processes are directly obtained from force measurements. It is shown that this specific energy is much less than of the rolling. The results also show that there is scope for optimizing the rolling schedules based on "minimum energy" as the objective function.

6.2. Model for rolling deformation and energy analysis

The steps in the estimation of the deformation component of the rolling energy are as follows. The thickness reduction in rolling is assumed to be accomplished by a plane-strain compression process in the rolling zone. **Figure 6.2** shows the rolling process model as plane strain compression, and description of key process parameters and model equivalents. The steps involved in the rolling pressure, force, torque and energy estimation are based on Dieter, Mechanical Metallurgy, 3rd Ed., 1986 and Schey, Introduction to Manufacturing Processes, 2nd Ed., 1987.

Steps involved in the energy estimation via roll torque:

a) Estimate rolling contact length and pressure
The deformation geometry is plane-strain compression adapted for the prevailing L/h regime. An appropriate yield stress is used based on the deformation conditions (hot vs cold working). The die-workpiece contact length L is assumed to be fixed throughout the process of thickness reduction, distinguishing this from the more conventional plane-strain forging/compression.

b) Estimate rolling force F (normal to the slab) as pressure x contact area.

$$Rolling\ Load,\ P = 1.15\bar{\sigma}Q_{fac}bL \tag{6-1}$$

where $L = \sqrt{R\Delta h}$ and $\Delta h = h_o - h_f$

c) Calculate torque as F x L/2 with lever arm as L/2.

$$\text{Torque} = \frac{\text{PL}}{2} \tag{6-2}$$

$$\text{Power (for 2 rolls)} = 2 * \text{Torque } * \omega = \text{ PL } \frac{\text{V}}{\text{R}} \tag{6-3}$$

d) Estimate specific energy of deformation (energy/volume of material rolled)

$$\text{Specific Deformation Energy } (\text{E}_{\text{def}}) = \frac{\text{Power}}{\text{vol. rolled/time}} = \frac{\text{PL } \frac{\text{V}}{\text{R}}}{\text{b}\bar{\text{h}}\text{V}}$$

Where $\bar{\text{h}} = \frac{\text{h}_0+\text{h}_\text{f}}{2}$, V = linear velocity

$$\text{E}_{\text{def}} = 1.15\bar{\sigma}\text{Q}_{\text{fac}}\frac{\Delta\text{h}}{\bar{\text{h}}} \tag{6-4}$$

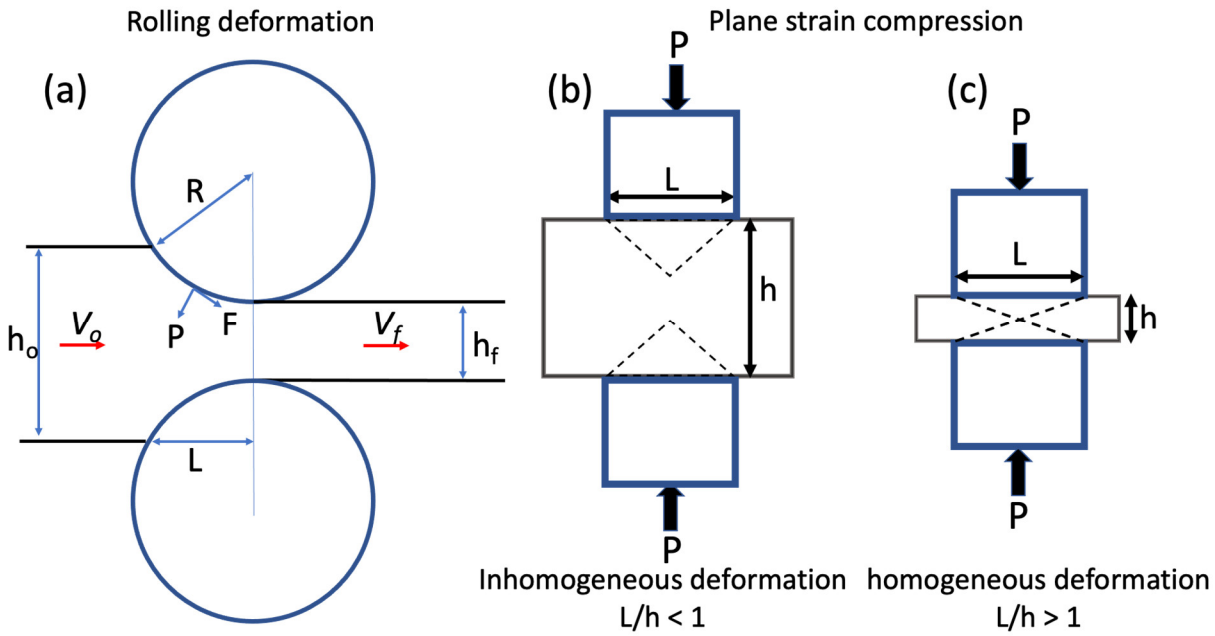

Figure 6.2 Schematic of rolling process and equivalent plane strain compression for both large and small h/L. L is the contact length between roll and workpiece in roll-gap and h (= 1/2(h_o + h_f)) is the mean sheet thickness in the process zone.

e) Determine the pressure multiplying factor, Q_{fac}

In the inhomogeneous deformation case, when h/L > 8.7, the deformation is similar to indentation of a semi-infinite body. For this case, it can be shown that pressure required for deformation is equivalent to three times the uniaxial flow stress of the material. However, if 8.7 > h/L > 1, the two deformation regimes begin to interact requiring less force to cause plastic deformation. The pressure multiplying factor (Q_{fac}) in this h/L regime, where non-homogeneous deformation prevails, can be read from the plot in **Fig. 6.3a**. The friction has negligible influence on the roll pressure and force.

When h/L < 1, the deformation is homogeneous (**Fig. 6.3b**). In this region, friction becomes a major contributing factor and the pressure multiplying factor (Q_{fac}) is governed by the well-known friction hill and can be determined from Eq. 6-5 as:

$$Q_{fac} = \frac{1}{\mu L/\bar{h}}\left(exp^{(\mu L/\bar{h})} - 1\right) \qquad (6\text{-}5)$$

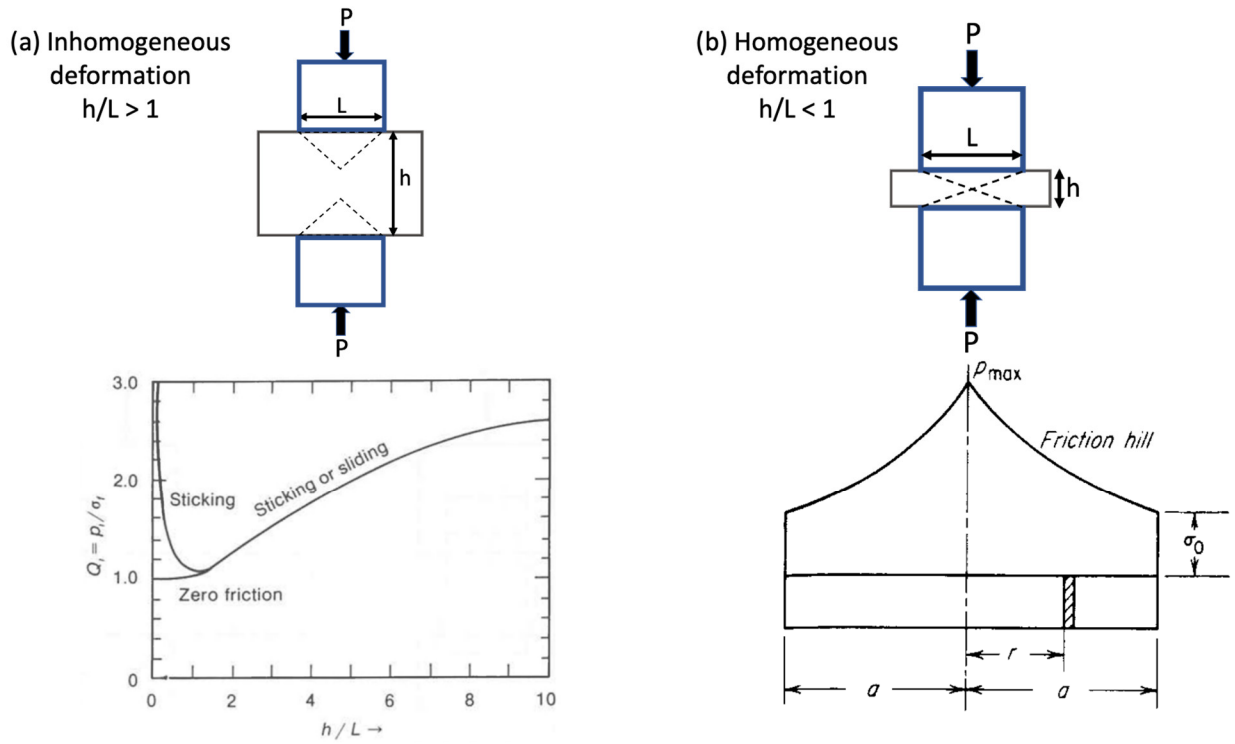

Figure 6.3 Determining the Q factor for a) inhomogeneous (friction unimportant) and b) homogeneous plane-strain compression (friction effect considerable).

f) Plane-strain compression modeling for estimating roll pressure and force

Hot rolling – Large h/L (two cases h/L > 8.7; and 0 < h/L < 8.7) corresponding to hardness testing and inhomogeneous plane strain compression in these two regimes. We use the latter model also for the h/L > 8.7 (hardness) regime as the difference in the rolling force is insignificant. The dominant factor influencing the deformation force and energy in hot rolling is inhomogeneous deformation. The friction effect on rolling force in these regimes is negligible because of the large slab thickness which makes the friction hill relatively flat. Strain-rate/temperature effects on yield strength, however, have to be incorporated.

Energy to heat the slab – $mCp\ \Delta T$

where m is mass of slab/ingot, C is specific heat of slab material and ΔT is the temperature rise of the slab due to the heating.

Total hot rolling energy = heating energy + deformation energy. For the specific energy estimation, we use the mass/vol (density) for m in Eq. 6-6.

$$E_{HR} = mC_p\Delta \boldsymbol{T} + \boldsymbol{C}\bar{\dot{\boldsymbol{\varepsilon}}}^{\boldsymbol{m}} \qquad (6\text{-}6)$$

Cold rolling Typically, in this regime h/L < 1. The force and energy are determined by homogeneous compression and the friction hill. The friction effect is now important, along with strain hardening in the deformation zone, in each rolling step. The cold rolling energy per unit volume is given by

$$\boldsymbol{E_{CR} = 1.15\left(\frac{\int_{\varepsilon_i}^{\varepsilon_j} K\varepsilon^n d\varepsilon}{\varepsilon_p}\right) * Q_{fac} * \frac{\Delta h}{\bar{h}}} \tag{6-7}$$

Where $\bar{\sigma} = \frac{\int_{\varepsilon_i}^{\varepsilon_j} K\varepsilon^n d\varepsilon}{\varepsilon_p}$, total strain in after the jth pass $(\boldsymbol{\varepsilon_j}) = \sum_0^N \boldsymbol{\varepsilon}$, initial accumulated strain in the ith pass $(\boldsymbol{\varepsilon_i}) = \sum_0^{N-1} \boldsymbol{\varepsilon}$ and strain per each pass $(\boldsymbol{\varepsilon_p}) = \boldsymbol{\varepsilon_j - \varepsilon_i}$

The total energy is obtained as the sum of the Hot Rolling energy and Cold Rolling energy.

$$E_T = mC_p\Delta T + C\bar{\dot{\varepsilon}}^m + 1.15\left(\frac{\int_{\varepsilon_i}^{\varepsilon_j} K\varepsilon^n d\varepsilon}{\varepsilon_p}\right) * Q_{fac} * \frac{\Delta h}{\bar{h}} \tag{6-8}$$

6.3. Specific energy results

The specific energy results obtained using the above analysis formulation are presented below in various forms so as to highlight individual energy contributions from hot and cold rolling, and workpiece pre-heating energy. Specific industry rolling schedules are concerned as well as model problems to illustrate parameter effects on energy.

Table 6-1: Typical industry rolling schedule for Al 6061 (or equivalent) alloy.

$\boldsymbol{Al\ 6061 - HR: C = 33\ MPa, m = 0.12, \dot{\varepsilon} = 155.7\ s^{-1},}$
$\boldsymbol{CR: n = 0, \sigma_y = 55\ MPa, K = 205\ MPa, constant\ \Delta h/pass}$

Process	Roll Diameter (mm)	Temp (K)	μ	h_o (mm)	h_f (mm)	Total Red. (%)	Total passes	Heating Energy (MJ/t)	Deformation Energy (MJ/t)	Total Energy (MJ/t)
Hot Rolling	1000	848	0.2	710	35.5	95	20	492.9	79.12	935.2
	600	623		35.5	3.55	90	3	291.3	71.84	
Cold Rolling	300	298	0.1	3.55	0.5	85	2	-	251.4	251.4
								784.3	402.34	1186.6

Table 6-2: Typical industry rolling schedule for 316 stainless steel.

HR: $C = 55\ MPa, m = 0.21, \dot{\varepsilon} = 385\ s^{-1}$,
CR: $n = 0, \sigma_y = 205\ MPa, K = 1254.8\ MPa, constant\ \Delta h/pass$

Process	Roll Diameter (mm)	Temp (K)	μ	h_o (mm)	h_f (mm)	Total Red. (%)	Total passes	Heating Energy (MJ/t)	Deformation Energy (MJ/t)	Total Energy (MJ/t)
Hot Rolling	1000	1473	0.2	710	35.5	95	20	822.5	78.47	1463.63
	600	1000		35.5	3.55	90	3.00	491.4	71.25	
Cold Rolling	300	298	0.1	3.55	0.5	85	2	-	519.31	519.31
								1313.9	669.04	1982.94

Table 6-3 Rolling process and material data for parametric studies.

h_o (mm)	h_f (mm)	Roll diameter, R(mm)	Yield Stress σ_y (Mpa)	K (MPa)	μ	n	Test case 1 Δh	Test case 2 $\frac{\Delta h}{h_o}$
9.6	0.55	300	55	205	0, 0.1 and 0.2	0, 0.1 and 0.6	Constant/ pass	Constant/ pass

Test Case 1 - Δh = constant/pass

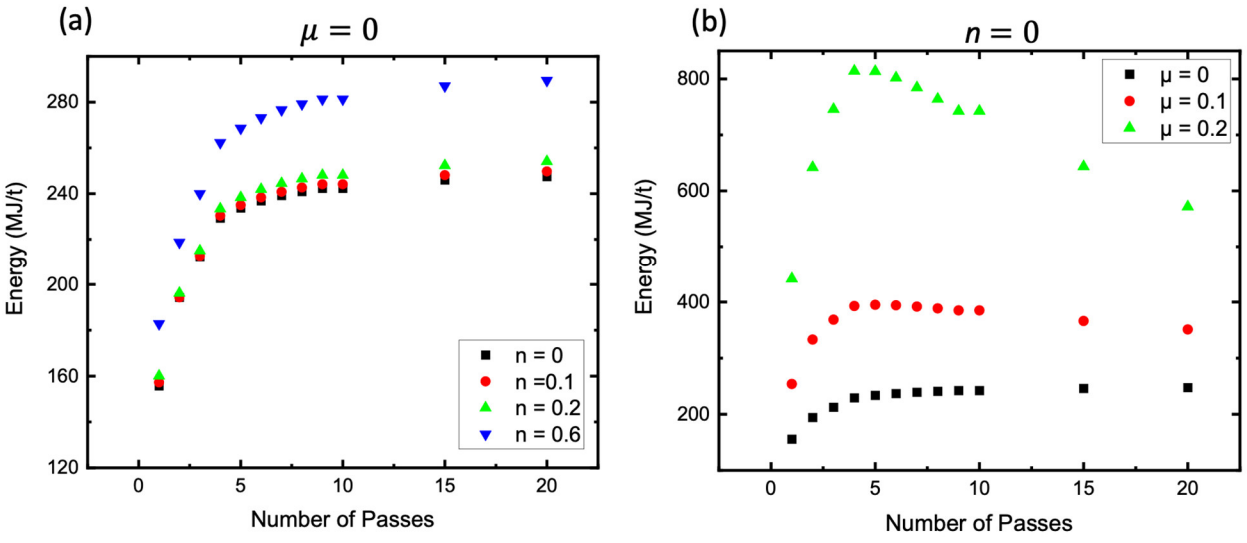

Figure 6.4 Dependence of specific energy on number of rolling passes. Rolling schedule - constant Δh per pass a) frictionless with various strain-hardening exponents, n, and b) perfectly-plastic material (n=0) and Coulomb friction.

Test Case 2 - Constant reduction/pass $\Delta h/h_o$

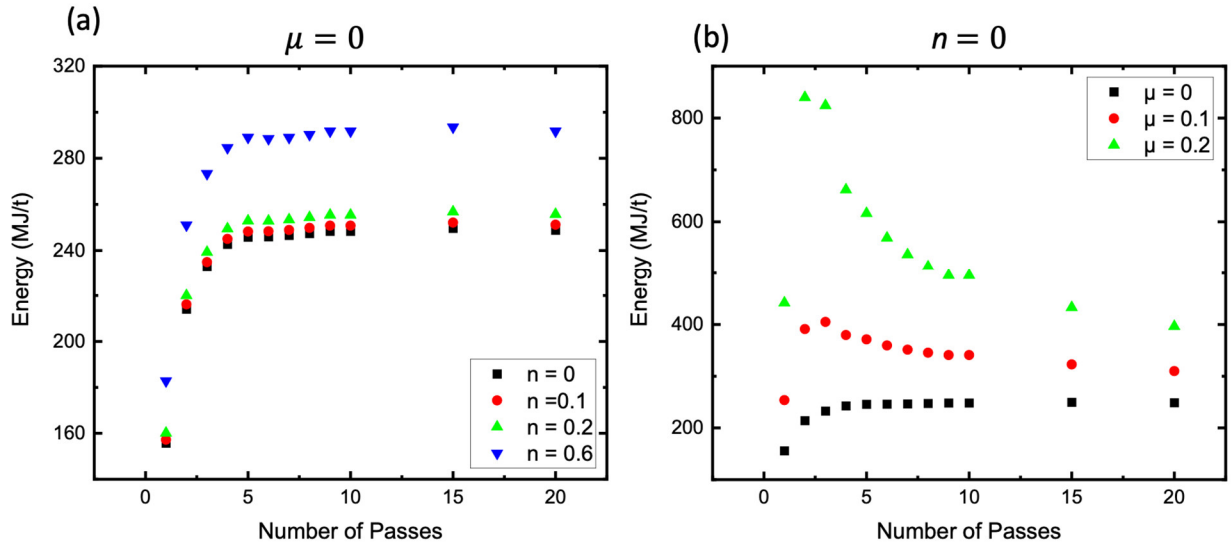

Figure 6.5 Dependence of specific energy on number of rolling passes. Rolling schedule - constant $\Delta h/h_o$ per pass a) frictionless with various strain-hardening exponents n and b) perfectly-plastic material (n=0) and Coulomb friction.

Test Case 3 - Combined effects of Δh and $\Delta h/h_o$

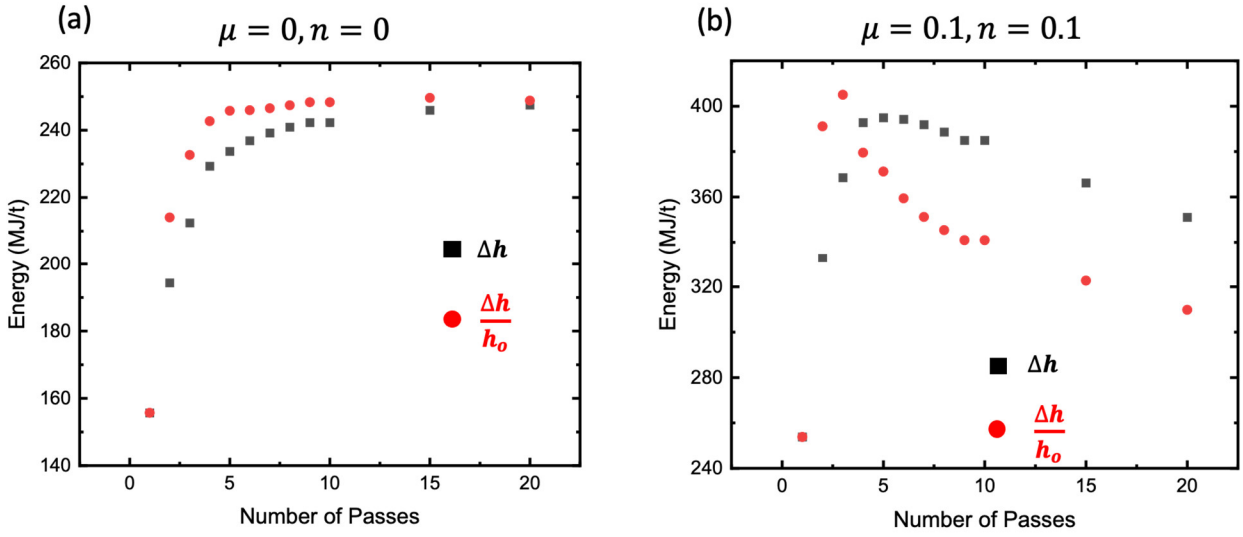

Figure 6.6 Dependence of specific energy on number of rolling passes. Schedules with constant Δh and $\Delta h/h_o$. a) frictionless and perfectly plastic material and b) Coulomb friction and strain hardening material.

6.4. Specific energy for strip production by the machining-based processing

We estimated the specific energy for the single-step strip production by the FM and HCE processes using direct measurements of the cutting force in lab-scale, machining-based strip production experiments. Al6061-T6 was the workpiece material used for comparing the specific energy of the machining-based deformation processes with that of rolling. A Kistler 3-component piezoelectric force dynamometer (coupled to the tool) was used to measure the forces. The natural frequency of the dynamometer in the as-mounted conditions was ~ 1 KHz, sufficiently high for accurate force measurement.

The experimental conditions, typical of machining practice for Al alloys, were as follows: Cutting speed V = 2 m/s; rake angle = 5 degs.; undeformed chip thickness t_o = 0.3 mm; deformed chip (strip) thickness t_c = 1 mm (FM), 0.5 mm (HCE); chip thickness ratio λ = 3.33 (FM), 1.67 (HCE). The measured cutting forces Fc were 1200 N (FM) and 1400 N (HCE). The specific cutting energy was obtained as, $E_{cutting}$ = Power/Material removal rate = FcV/Vt_o(strip width = 6.35 mm).

Based on the measured cutting forces and parameter values, $E_{cutting}$ was obtained as 233.3 MJ/ton (FM) and 272 MJ/ton (HCE). It is clear upon comparison with Table 6-1, that these energy values are substantially smaller than the corresponding specific energy value of ~ 1180 MJ/ton for rolling of Al6061 strip. In fact, the HCE and FM energy values are < 25% of the rolling energy. This confirms our hypothesis that the single-step production of strip and sheet by the machining-based deformation processes is highly energy-efficient compared to the rolling.

6.5. Conclusions

1. An energy analysis framework has been established for rolling of sheet and foil
2. Specific energy for rolling of Al and stainless steel alloy sheet has been estimated for typical industry schedules
3. The rolling specific energy is seen to be quite large. Both workpiece heating energy (~ 60 to 70%) and deformation energy (30 to 40%) are significant in rolling. Hence the conclusions reached by Fruehan *et al.* (2000) about the deformation energy contribution being not significant have to be revised.
   (Note: The above specific energy estimates for the rolling are only a lower bound – this is because idle roll-motor power and losses, material wastage, intermediate annealing (heating) energy contributions etc. have been neglected. The idle power and annealing energy contributions in particular are expected to be considerable, as much as 50% of the overall specific energy).
4. Parametric studies have been made of the effect of friction, strain-hardening and number of passes on rolling specific energy. These studies show that a) the specific energy peaks at or near $\mu^2 R$ (maximum reduction/pass) and b) the friction has much larger effect on the energy than the strain hardening (n).
5. The specific energy for strip production by the single-step machining based processing is < 25% of that for the rolling.

Ongoing and future work is focused on improving the specific energy estimates; characterizing the specific energy for a broad range of alloys; and calculating carbon footprint and emissions associated with the rolling plant and the machining-based processing.

7. Formability and Stampability

The Pacific Northwest National Labs team characterized the mechanical properties of high-silicon electrical steel strips produced by Purdue's hybrid cutting-extrusion (HCE) process and compared the properties against commercially available strips. The main application area of the strips is the core of electric motors, transformers, and generators, where the strips are stamped into small pieces and laminated to build the core. Mechanical properties relevant for this application are determined as formability and stampability. Therefore, the work at PNNL was divided into two tasks. In the first task, formability was determined by bending the strips over a known radius. This test also gives an indirect measure of the ductility of the strips. In the second task, a stamping process was simulated through punch tests. Punch tests were used to determine the edge quality of the stamped pieces, which is a critical parameter in the lamination efficiency for the electric motor core application.

7.1 Materials and methods

Materials Commercial strips (Cogent No. 7 / Sura No. 18) for benchmarking were supplied from Polaris Laser Laminations LLC, West Chicago, IL. They were produced by Cogent Power – Surahammars Bruks AB, Surahammars, Sweden. Composition of the strips was: <0.003 % C, 3.01 % Si, 0.21 % Mn and 0.44 % Al, all weight %, balance Fe. The strips were cut from the cold-rolled stock with 0.18 mm thickness both parallel and perpendicular to the rolling direction. The strips were non-grain-oriented but fully processed, i.e. annealed, to obtain the desired magnetic properties. **Table 7-1** lists some of the typical and measured properties of the strips. Detailed specifications of the strips are also available at Cogent Power.

Table 7-1 Mechanical, Electrical and Magnetic Properties of the Commercial Strips

Property	Value
Typical Core Loss at 50 Hz (1T)	1.00 W/kg
Measured Core Loss at 400 Hz (1T)	11.7 W/kg
Resistivity	52 μΩ.cm
Typical Yield / Tensile Strength	370 / 450 MPa

Purdue University supplied shear processed strips for formability and stampability testing in two batches. First batch had strips produced by free machining and subsequent cold rolling had a width and thickness of 48 mm and 0.20 mm. Strip produced by HCE and subsequent cold rolling was 20 mm wide and 0.31 mm thick. Both strips were in as-processed condition with some intermediate annealing between the machining and cold-rolling steps. Cold rolling was performed to obtain the desired surface finish. Second batch was fully-annealed strips that were produced either by free machining + cold rolling (FM) or HCE + cold rolling. FM strip was 14.8 mm wide and 0.31 mm thick and HCE strip was 17.1 mm wide and 0.32 mm thick.

Formability testing Formability of the annealed strips were evaluated by both with V-block bending (90°) and 180° bend and flatten tests in accordance with the ASTM E290 standard. Top and bottom orientations in the tests respectively refer to the constraining tool (or free surface) and cutting tool sides of the strips during processing (**Fig. 7.1**). As the top surfaces of the strips were rougher and sometimes contained micro-cracks compared to the bottom surfaces, both surfaces were placed under tension during the bend tests. The result of this test is r/t ratio, which is defined as the minimum inside radius of curvature (r) that is necessary to form a bend in a strip of thickness (t) without failure. Smaller values indicate higher formability. For a given material, this ratio also depends on the initial thickness and it decreases as the test material gets thinner. While bends that are greater than or equal to 90° are recommended, r/t ratio is independent of the bending angle. Also, it can be linked to the ductility of the test material.

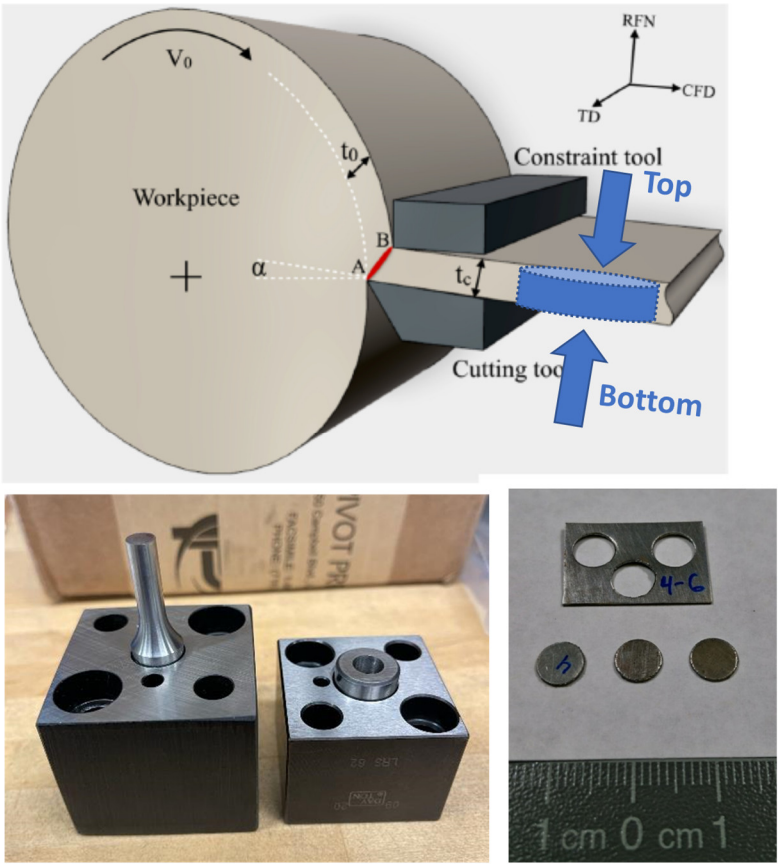

Figure 7.1 (left) Schematic for the punching of the Purdue strips relative to strip process faces and (right) actual punched discs from the Purdue strips.

Stampability Tests and Edge Quality Characterization Stampability of commercial and HCE strips were tested with a punch test apparatus (Figure 1) mounted in a universal testing machine. Overall, ~ 10 discs with 6.35 mm diameter were punched from each strip. Clearance between punch and die was 0.019 mm on each side, corresponding to about 11% of the commercial strip thickness of 0.18 mm. This value is in line with the recommended value for high-silicon steel strips

with tensile strength of ~450 MPa. Discs were punched from both surfaces of the strips (**Fig. 7.1**) to test any variability due to the surface finish and orientation. Spacing between each punch was adjusted in a way that there was no interference between successive punches (**Fig. 7.1**). Force and displacement data were recorded during all tests. With the measurement of the forces, it was possible to calculate the shear yield and tensile strength of the strip through the following equation:

$$\tau = \frac{P}{2\pi r_{avg} t} \tag{7-1}$$

where $r_{avg} = \frac{r_{punch}+r_{die}}{2}$. The shear strength values are necessary for the design of the large-scale stamping process.

Sheared edges of the punched forms contain features such as rollover, burnish, and fracture surfaces, which are common in stamping of sheets and they are controlled by the overall fracture behavior of the punched material (**Fig. 7.2**). Among the fractured edge features, one of the most important and relevant for electric motor application is the burr height. It determines the edge quality and therefore the lamination efficiency of the stamped disks. Lower burr height is desired for the higher lamination efficiency, which decreases the core losses in an electric motor and increases its efficiency.

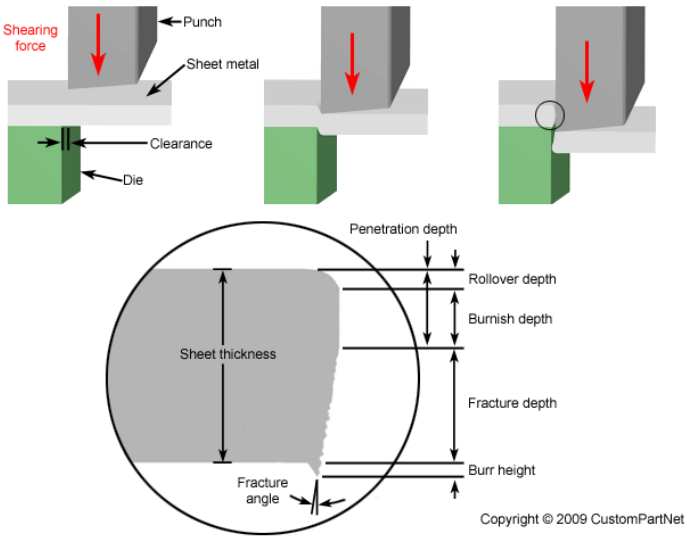

Figure 7.2 Features determining the edge quality of the stamped strips (CustomPartNet)

Another relevant edge quality feature is the level of residual deformation at the sheared edges. Various studies in the literature show core losses of up to 20% due to the deformed edges of the stamped strips. The deformed edges adversely affect the magnetic properties. **Figure 7.3** is an example from such studies where the electrical steel strips were punched with tools having various sharpness. Sharper tools result in clear edges, minimal burr formation and less deformation at the edges, whereas blunt tools result in burrs and deformed grains at the edges. Strips punched with sharper tools had better magnetization behavior in this study, which is consistent with the other observation in the literature. They had lower iron losses and magnetic field demand for reaching a certain level of induction decreased.

Electron backscatter diffraction analysis (EBSD) were performed in a scanning electron microscope to image the level of deformation at the edges of the strips punched in this study. Punched discs were sliced in half and were mounted on the cross-section and mechanically polished at PNNL. Polishing was enough to both remove the deformation from cutting operation and obtain the desired surface finish for the EBSD analysis. The samples were then shipped to

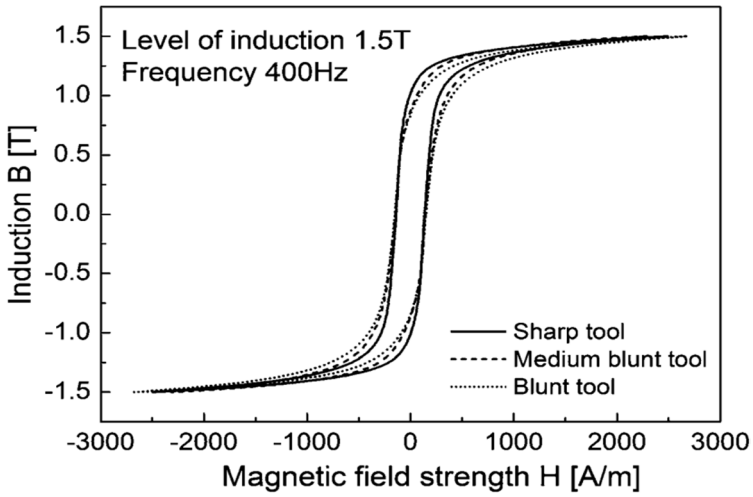

Figure 7.3 Effect of punch sharpness on the magnetization of the stamped strips (after Harstick, Ritter, and Riehemann)

Purdue University for the EBSD study, which gave the grain size, texture, and dislocation density at the deformed edges as well as the center regions of the punched discs.

7.2 Formability Results

Overall, the strips are very formable with rare cracking when top surfaces were under tension. It was possible to reach tighter bend radii with the 180° bend and flatten tests. The bend radii of 0.07 and 0.13 mm resulted in r/t = 0.41 for the commercial and r/t = 0.50 for the as-processed HCE strips (Figure 4). These ratios are on par with highly formable cold-rolled steels with r/t ~ 0.5-1. As the strips were cracking during unfolding, these ratios can be assumed as the upper-bound of formability and they are indicative of excellent formability. With these ratios, most of the forming operations can be performed on both strips without any issues.

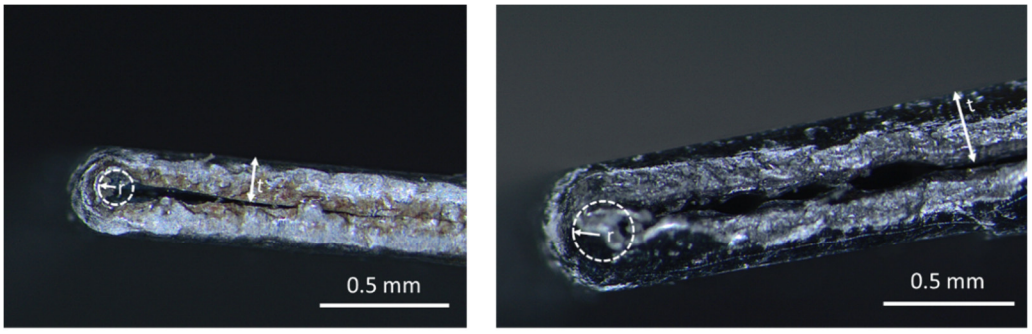

$\bar{r} = 72\ \mu m$
$\bar{t} = 177\ \mu m$
$\frac{r}{t} = 0.41$

$\bar{r} = 134\ \mu m$
$\bar{t} = 270\ \mu m$
$\frac{r}{t} = 0.50$

Figure 7.4 Side view stereomicroscope images of 180° bent strips; (left) commercial, (right) as-processed HCE. Note that the thicknesses measured by microscopy are slightly lower than the nominal thickness of the strips.

Table 7-2 lists a selection of formability test results for both annealed FM and HCE strips. Highest r/t (minimum bend radius ratio) before cracking is 1.30 for the HCE strip. This can be assumed as the lower bound for the formability, which happens when the top surface is under tension. However, top surface being under tension does not necessarily indicate failure as some strips were formable even when their top surfaces was placed under tension during 180° bend and flatten tests. A such example HCE strip listed in Table 2 reached the lowest r/t ratio of 0.23 and demonstrated highest formability even when its top surface was under tension during 180° bending. Both FM and HCE strips reached similar r/t ratio of ~ 0.3 under 180° bending without failure (**Fig. 7.5**). A FM strip 180° bent with its top surface under tension cracked at r/t = 0.38 (**Fig. 7.5**), which can be assumed as the upper formability limit of the Purdue strips. This ratio is similar to that of the commercial strip, r/t = 0.41. Both the commercial and Purdue strips also reached similar minimum bend radii of ~ 0.07 mm, independent of their starting thickness. As a summary, Purdue strips have comparable formability to the commercial strips. However, there is a rare risk of cracking of the Purdue strips due to their uneven surface finish, especially when the top surfaces are under tension during bending.

Table 7-2 Formability test results of some selected strips and test conditions

Sample	Radius Measured (mm)	r/t	Failure (Yes or No) according to ASTM E290
FM top 90 deg	0.910	2.94	No
FM bottom 180 deg	0.089	0.29	No
FM top 180 deg	0.117	0.38	Yes
HCE top 90 deg	0.417	1.30	Yes
HCE bottom 180 deg	0.088	0.28	No
HCE top 180 deg	0.073	0.23	No
Commercial 180 deg	0.072	0.41	No

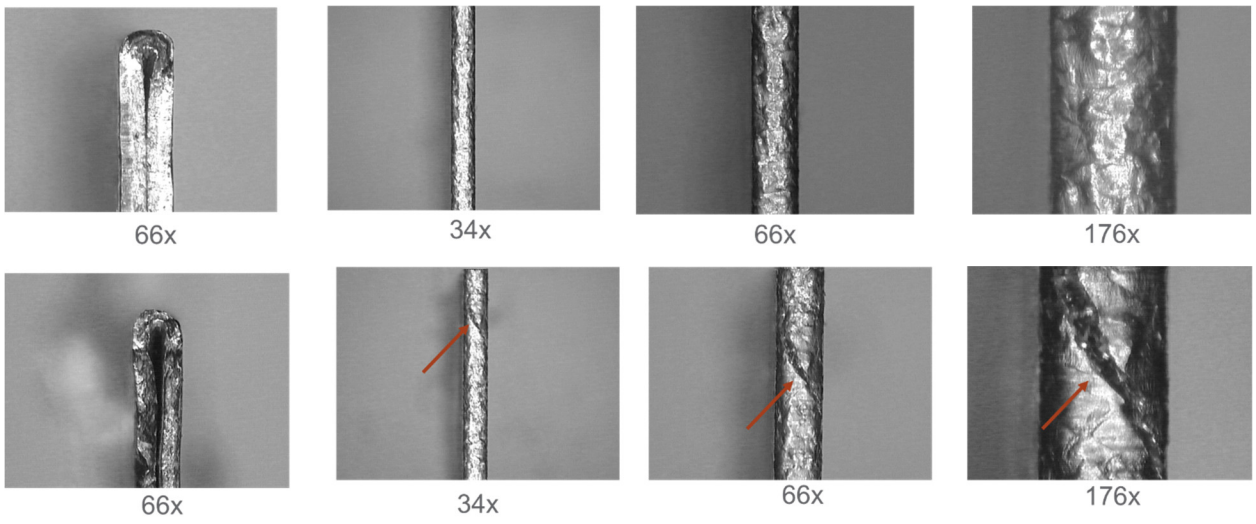

Figure 7.5 Pictures of 180° bent strips: (top row) HCE bottom, r/t = 0.28, no failure; (bottom row) FM top, r/t = 0.38 cracked (marked by arrows).

7.3 Stampability Results

Punching of the commercial strip was successful and the discs can be punched without any issues. The punched discs retained their good surface finish with minimal edge damage. **Figure 7.6** shows the top and bottom face of a representative punched disc. Edge damage in the form of a minimal burr is not visible in this image and it is measured by optical microscopy. Force-displacement behavior during punching was also repeatable and the average punching force was 150 kgf (**Fig. 7.6**).

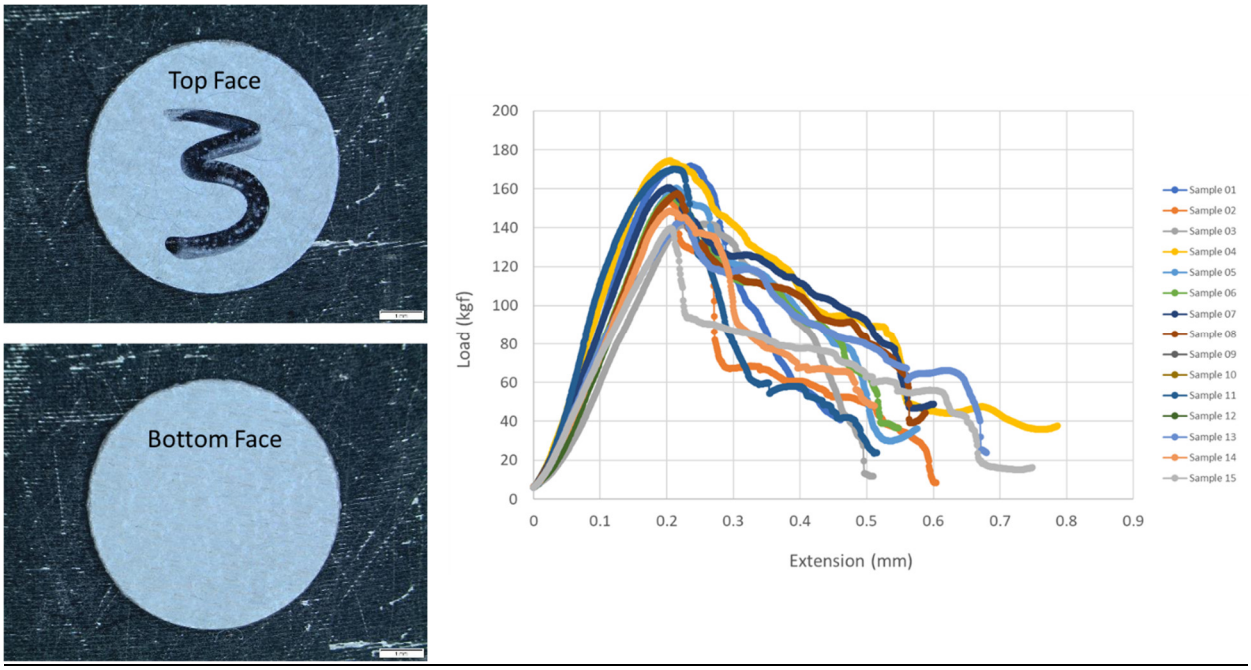

Figure 7.6 Pictures of the punched discs from the commercial strip (left) and force-displacement data recorded during the punch tests (right). Scale bars are 1 mm.

As-processed Purdue HCE strip has stampability comparable to the commercial strip. There were no issues in punching the discs. Edge quality was also similar to the commercial strip. Punching orientation did not make a difference and punching from either of the surfaces produced discs with similar appearance and edge quality. Surface quality of the punched discs was slightly worse than the commercial as there was slight opening of the serrations on the constraint face of the strip during stamping (**Fig. 7.7**). Force-displacement data were repeatable, and the average maximum punching force was 320 kgf as the Purdue strips were thicker and they had prior cold work (**Fig. 7.8**). Despite the amount of prior cold work, it was possible to observe some strain hardening in the force-displacement curves, indicative of ductility in this strip. Displacements at the maximum punch force matched the strip thickness.

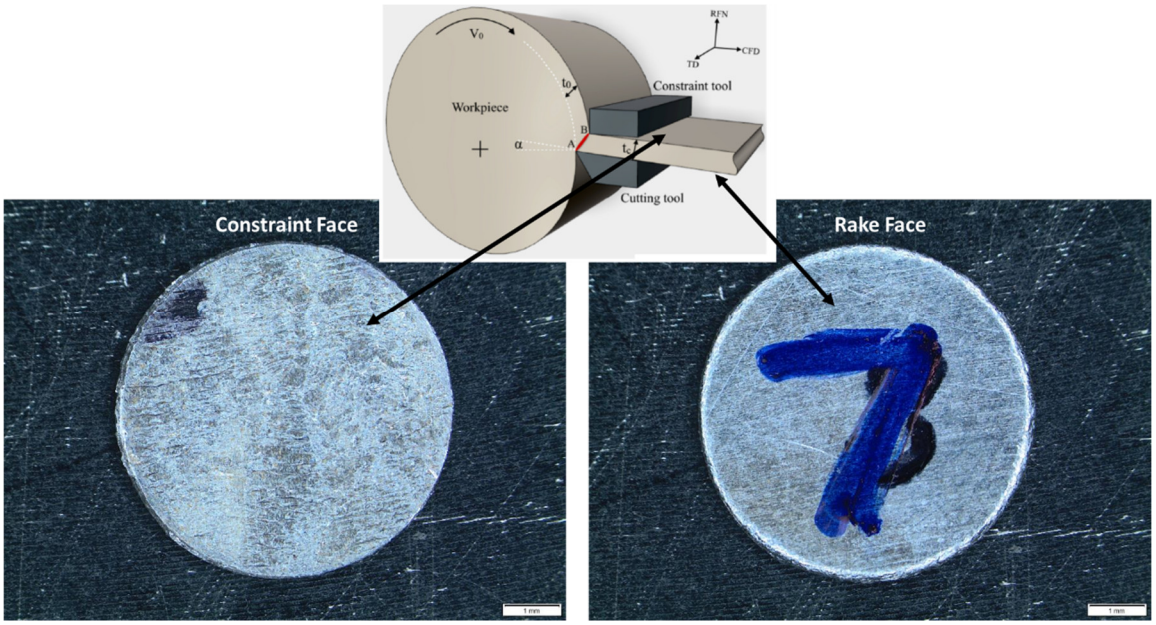

Figure 7.7 Pictures of the punched discs from the Purdue HCE strip. Scale bars are 1 mm.

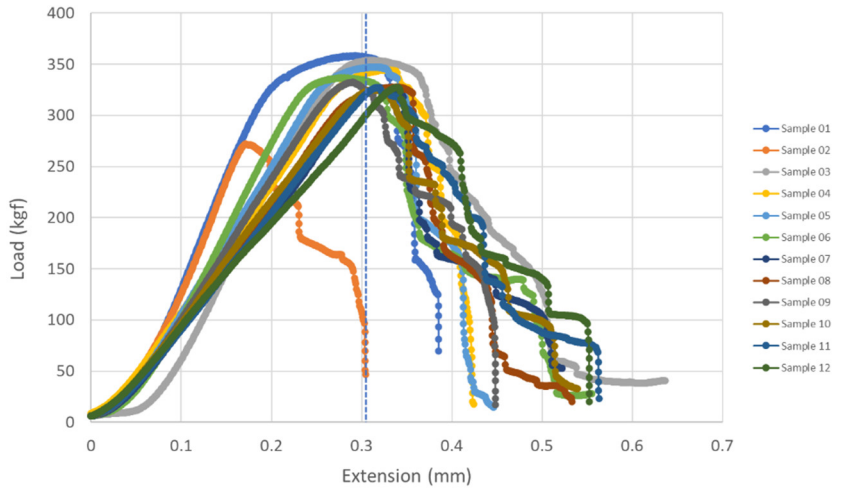

Figure 7.8 Force-displacement curves of the discs punched from Purdue HCE strip.

Annealed Purdue strips were also stampable independent of their testing orientation. There was no cracking in any of the test and the punched discs had clean and sharp edges with minimal burr formation. **Figure 7.9** shows examples of such discs and their starting strips.

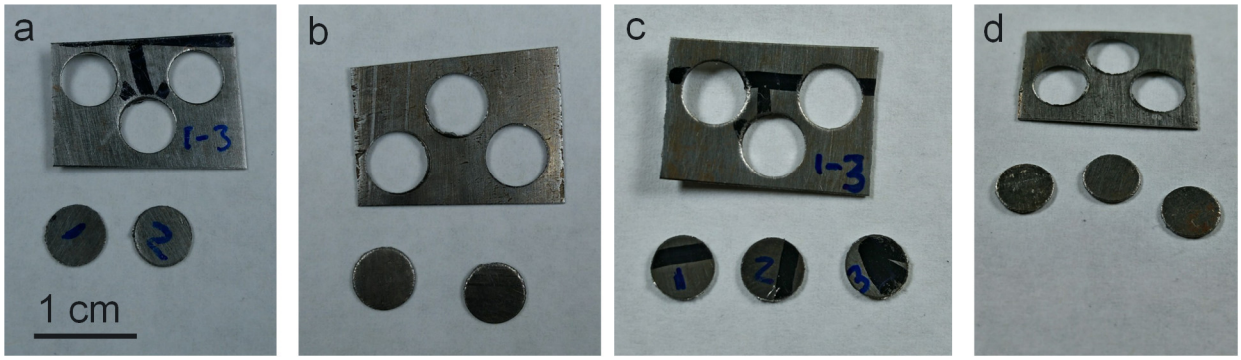

Figure 7.9 Pictures of the stamped discs and their starting strips: (a & b) annealed HCE strip stamped from its bottom surface; (c & d) annealed FM strip stamped from its top surface.

Force and displacement curves were also repeatable for a given strip, independent its testing orientation (**Fig. 7.10**). HCE strips required and average stamping force of ~ 320 kgf, whereas FM strips required a lightly lower force of ~ 300 kgf. The slight difference is consistent with the thickness variation between the strips. Strips may also be recrystallized to different levels and this can be another factor responsible from the slight difference. Both strips also reach their maximum force at about their corresponding thickness.

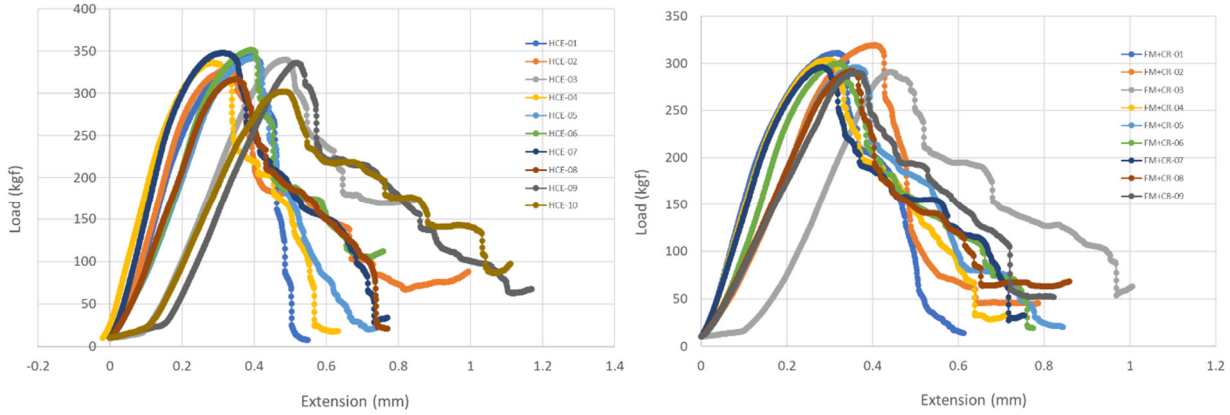

Figure 7.10 Force-displacement curves of the stamping tests: (left) HCE; (right) FM.

When normalized with their thickness, punch forces become similar for both of the Purdue strips (**Table 7-3**). These values are slightly lower than the values before annealing but still higher than that of the commercial strip. Shear strengths of the annealed strips are also lower than the as-processed consistent with their recrystallization level. It is important to note that even as-processed strips were recrystallized to some extent due to the intermediate anneals during its processing. Except the slightly higher punching force, Purdue strips are as stampable as the commercial ones without any issues.

Table 7-3 Stampability characteristics of the commercial and Purdue strips.

	Punch Force/Thickness (N/mm)	Shear Strength (MPa)
Commercial	8655	217.1
Purdue HCE before annealing	10126	253.9
Purdue HCE annealed	9806	245.9
Purdue FM annealed	9490	238.0

7.4 Edge characterization

Figure 7.11 shows the mounted cross-section of the punched discs from the commercial and as-processed Purdue HCE strips. Commercial strip appears to be little bent after punching but this can be due its lower thickness compared to the Purdue HCE strip. Both strips appear to be recrystallized as the grains were visible even after polishing. Recrystallization in the commercial strip is expected as it was fully annealed, whereas recrystallization in the Purdue strip can be due to the intermediate annealing between the machining and cold-rolling steps. Grain size of the Purdue strip appears to be bigger than the commercial. Optical images were also recorded from the annealed Purdue strips (not shown here). They are fully recrystallized as expected from the annealing operation.

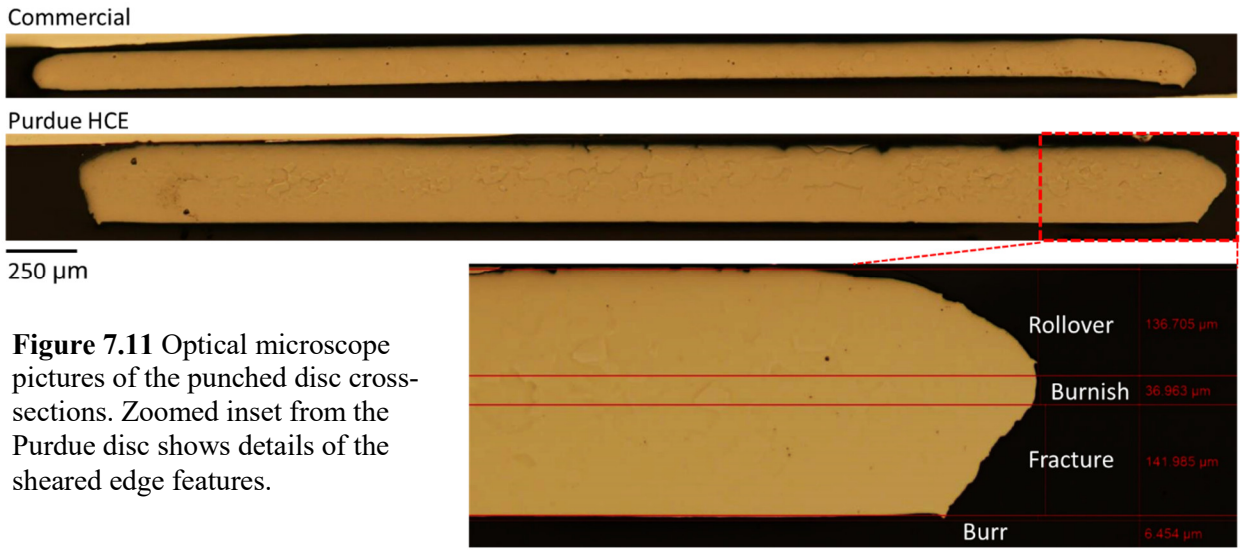

Figure 7.11 Optical microscope pictures of the punched disc cross-sections. Zoomed inset from the Purdue disc shows details of the sheared edge features.

The punched discs usually show the typical features of punching (**Fig. 7.11**). In some cases, rollover was too deep without the formation of burnish. Also, in some cases there was no visible burr. **Table 7-4** summarizes the average values of punching features as a fraction of the strip thickness. Burr height was taken as zero and included in the averages for the cases without a visible

burr. Rollover and burnish depths were added together and then averaged. In both commercial and Purdue strips, majority of the sheared edge is rollover and burnish. Commercial and Purdue FM+CR annealed strips show similar burr height and fracture depth fractions. These are the results of higher amount of plastic deformation and ductile fracture during punching of these strips. Both HCE strips, whether as-processed or annealed, have higher fracture depth and smaller rollover and burnish fractions compared to the commercial strips. Despite the higher fraction of fracture depth, Purdue strips have lower burr height fraction. These results are an indication of a more prominent brittle-type fracture in the HCE strips. The strips deform less during the punching and fails by fracture with lower burr height fractions. Absolute values of the average burr heights are similar for both strips: 7.8 µm for commercial and 7.0 µm for Purdue HCE, 7.9 µm for Purdue HCE annealed which are higher than the typical coating layer depth of ~ 1.5 µm.

Table 7-4 Comparison of punching features as a fraction of strip thickness for commercial and Purdue samples.

% of sheet thickness	Rollover Depth	Burnish Depth	Fracture Depth	Burr Height
Commercial	**70%**		**30%**	**4.4%**
Purdue HCE	**56%**		**41%**	**2.3%**
Purdue HCE Annealed	**60%**		**37%**	**2.5%**
Purdue FM+CR Annealed	**41%**		**24%**	**4.8%**

Importance of burr height in determining the lamination efficiency is shown in **Fig. 7.12**. This sketch simplifies the lamination case with following assumptions: 1) no coating on the strips and 2) uniform burr height in the punched form. Then the lamination efficiency is: 100 % of the gap, where % gap is calculated as:

$$\%\ of\ gap = \frac{(n-1)x}{nt} x100. \quad (1)$$

In this equation n is the number of laminated layers, x is burr height, and t is the strip thickness. The gap in the laminated stack is directly proportional to the fraction of burr height to strip thickness (x/t). Commercial strips have a typical lamination efficiency of 96%, corresponding to 4% gap when laminated, neglecting the gap originating from coatings. With x/t results reported in **Table 7-1**, Purdue HCE strips will have half of the gap (2%) compared to the commercial strips (4%), resulting in 98% lamination efficiency. This increase will certainly reflect as efficiency increases in electric motor applications due to smaller core losses.

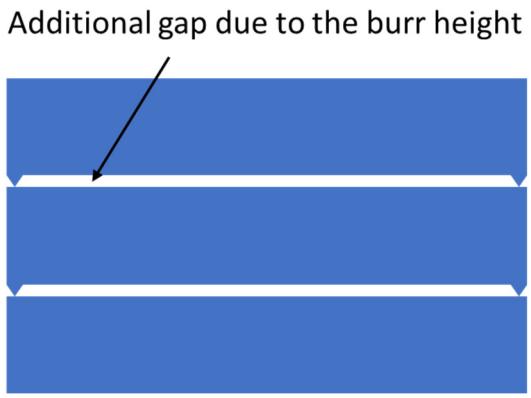

Figure 7.12 Sketch showing the contribution of burr height to the gap between the laminated strips.

Edge deformation behavior of commercial strips and Purdue strips are also different. EBSD orientation map images and associated dislocation density maps from the edges of each strip show a drastic difference (**Fig. 7.13**). The commercial strip has deformation localized around the burr with high dislocation density regions (shown by red color in the dislocation maps) extending into the strip. The as-processed HCE strip, on the other hand, shows a more uniform distribution of deformation with some high-density dislocation regions along the whole edge. In this case, area of high-density dislocation regions is considerably smaller compared to the commercial sample. Annealed HCE sample has dislocation accumulation around the burr and the edges, but the dislocation density is again lower than the commercial sample. Among all three samples, as-processed HCE sample shows the minimum amount of deformation, and this is consistent with its minimal burr formation and brittle-type fracture behavior. Both the commercial and annealed HCE strips have significant plastic deformation near the edges, however intensity is higher in the commercial sample. This plastic deformation results in the burr formation. Combined with the minimal burr formation, limited amount of plastic deformation in HCE strips should results in better magnetization and lower core losses.

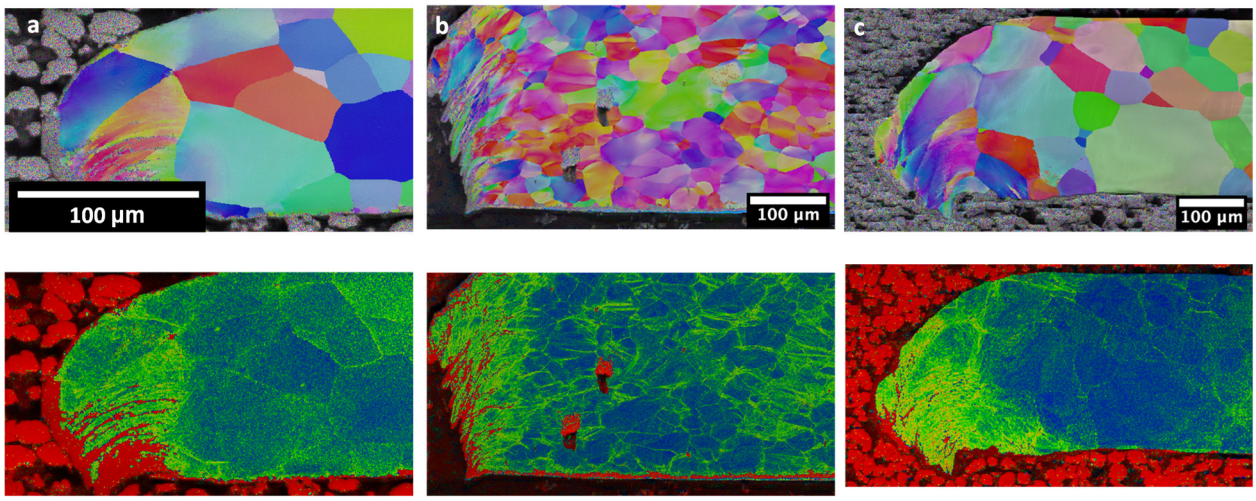

Figure 7.13 EBSD grain orientation and dislocation density maps for: (a) commercial, (b) as-processed HCE, and (c) annealed HCE samples. Note that strip thicknesses and the corresponding scale bars are different.

7.5 Summary

Purdue strips produced by hybrid cutting extrusion and free machining methods are tested to evaluate their formability and stampability performance and compared against a commercial strip. Purdue strips are as formable as the commercial strip, especially in their annealed condition. They are able to reach the same or better *r/t* ratios during 90 and 180^{o} bend tests. There is a rare risk of cracking of the Purdue strips due to their uneven surface finish, especially when the top surfaces are under tension during bending.

Both the commercial and Purdue strips are stampable. Discs, or any circular geometry, can be punched from either of the strips without any issues. Strip orientation does not matter during stamping and both strips produce successful punched discs without any cracking or distortion. The punching force/thickness and shear strength of the Purdue strips are slightly higher due to the prior cold work and higher silicon content in these strips. Edge quality of the discs punched from the Purdue strips is better compared to the discs punched from the commercial strips. Purdue discs are straighter, show features of the desired brittle fracture with lower burr height. The HCE strip in the as-procced condition has the best edge quality and minimum burr height with respective to its thickness. The lamination efficiency without any coatings is shown to be directly proportional to the burr height to thickness ratio and the lower ratio in Purdue strips may result in a smaller gap between the strips when laminated. Calculations show that laminated Purdue strips have potential in achieving 2% gap compared to the 4% typical gap in the laminated commercial strips.

These results indicate that the Purdue strips are suitable for producing laminations used for electric motors and have potential to achieve better magnetic performance due to their higher edge quality.

8. Key Findings

The goal of the present project was design and demonstration of a new energy-efficient prototype process for producing high-Si electrical steel strip of commercial widths and thickness, and with superior electrical and magnetic properties than current electrical steels (Fe-3.2% Si as benchmark). The potential applications domain for these steels is electrical motor core laminations.

We have addressed this goal by accomplishment of the following specific objectives and tasks outlined in the SOPO.

a) An Fe-4Si-4Cr alloy containing 4% by weight each of Si and Cr was developed as the bulk workpiece material for conversion to sheet and foil forms. The alloy had electrical resistivity > 80 μΩ-cm, induction flux density > 1.48 T at 5000 A/m and core loss 35% lower than the benchmark Fe-3.2% Si alloy. The alloy meets DOE target specifications for motor core attributes. The design of the alloy was guided by the following considerations: the Si content controlled for the electrical properties and the Cr content tailored to meet material/process workability requirements.
b) A unique machining-based deformation processing system was designed and scaled-up to produce strip of commercial width (25 mm to 150 mm) and thickness (up to 0.5 mm) from the Fe-4Si-4Cr alloy; and other alloys of varied workability including copper, Al6061-T6 and naval brass. The key attributes of the machining-based strip production are deformation processing by concentrated simple-shear; single-step production of strip from ingot using

compact machine infrastructure; strip surface finish of Ra 0.35 to 1 micrometer that is comparable/superior to that of rolled strip; discrete production of strip that can potentially be done at point of use; and controllability of strip mechanical/formability properties by deformation control.

c) The electrical, magnetic, surface quality, mechanical, formability, and metallurgical properties/attributes of the machining-based strip were established by direct ASTM standard tests or equivalent measurement techniques.
d) Punching characteristics of the strip in terms of load, edge quality and macro defects were similar to those of conventional 3.2% Si electrical steels. These punching characteristics are critical from a manufacturability perspective for motor/transformer core applications.
e) A modeling framework for energy analysis of multistage rolling and the machining-based deformation processing has been established. Application of this modeling to the two strip-making processes (rolling and machining-based) showed that the machining-based process requires significantly lower specific energy for processing, only ~ 25% of that for rolling. The energy estimates were obtained by simulation of industrial rolling schedules for the rolling process, and from direct measurements of cutting forces (the power component) for the machining-based strip production. The deformation modeling framework established can be adapted for a range of sheet-metal forming, bulk metal forming, and machining processes. It can also be used to identify the key process parameters that control process specific energy. The inputs to the process model can be obtained from published data, processing handbooks and small-scale lab experiments.
f) A comparative analysis of advantages and disadvantages of machining-based processing against rolling for strip production has been carried out and tabulated.

The single stage machining-based processing, with compact infrastructure, represents a new manufacturing paradigm for sheet and foil manufacturing that can potentially also be applied to advanced titanium, aluminum and magnesium alloys.

The goals and objectives were accomplished by a cross-disciplinary project team comprising of personnel from Purdue University; M4 Sciences LLC, a small-business focused on advanced manufacturing technology development; the Pacific Northwest National Labs; and tool and metals manufacturers. The team is currently in advanced discussions with multiple entities – companies, venture fund – for future process development for commercialization.

9. Acknowledgements

We would like to acknowledge Steve Sikirica, Gibson Asuquo, Colleen Lipps and John Harrington, all program officers of the DOE, for important technical and administrative inputs throughout the entire course of the project. Their comments, suggestions and encouragement were valuable, and contributed in no small measure to project progress towards the milestones.

We would like to thank Dr. Rachid M'Saoubi of Seco Tools (Fagersta, Sweden) for providing the large-scale tungsten carbide tools used in the project, free of charge, and for additional technical consultations. Thanks are also due Dr. Andrew Kustas of the Sandia National Labs for discussions and suggestions pertaining to soft magnetic alloys.

Discussions with various metals manufacturers including AK Steel, Nucor Corp. and Prysmian General Cable are gratefully acknowledged. We would like to thank the Haynes International, Kokomo, IN for providing access to forging facilities for workpiece preparation.

10. Products

1. H. Yeung, K. Viswanathan, A. Udupa, A. Mahato and S. Chandrasekar. “Sinuous Flow in Cutting of Metals,” *Physical Review Applied*, 8, 054044, 2017. doi: 10.1103/PhysRevApplied.8.054044

2. A. Udupa, K. Viswanathan, M. Saei, J. B. Mann and S. Chandrasekar, “Material-Independent Mechanochemical Effect in the Deformation of Highly Strain-Hardening Metals,” *Physical Review Applied*, doi: 10.1103/PhysRevApplied.10.014009. 2018, Featured in APS Physics Focus with commentary by Phillip Ball, eminent science writer. Video on topic has received more than one million views on YouTube.

3. B. S. Puentes Rodriguez, D. Brice, J. B. Mann, S. Chandrasekar, and K. Trumble, “Production of High-Resistivity Electrical Steel Alloys by Substitution of Si with Al and Cr,” in *TMS 2019 148th Annual Meeting & Exhibition Supplemental Proceedings*, Springer, 2019, pp. 599–606. doi.org/10.1007/978-3-030-05861-6_57

4. US Patent Application 16/681,480, Methods of Sheet Metal Production and Products Produced Thereby, X. Bai, J. B. Mann, K. P. Trumble and S. Chandrasekar, Filed November 12, 2019. Published US 2020/0188972 A1, June 18, 2020. Disclosed on iEdison invention report.

5. D. Sagapuram, A. Udupa, K. Viswanathan, J. B. Mann, R. M’Saoubi, T. Sugihara and S. Chandrasekar, “On the Cutting of Metals: A Mechanics Viewpoint” Invited: *ASME Journal of Manufacturing Science and Engineering,* 142(11), p. 110808 (2020). doi: 10.1115/1.4047869.

6. K. Trumble, S. Puentes, M. Issahaq, M. Saei, A. Udupa, J. B. Mann and S. Chandrasekar, “Hybrid Cutting-Extrusion for Sheet Metal Production with Exceptional Microstructure Control,” Invited conference presentation, TMS 2020 Annual Meeting, San Diego, CA, 23 February 2020.

7. B. S. Puentes, J. Mann, S. Chandrasekar and K. Trumble, “Production of Strips of Low-Loss Soft Magnetic Alloys by Cutting Processes,” Conference presentation, TMS 2020 Annual Meeting, San Diego, CA, 23-27 February 2020.

8. A. Udupa, K. Viswanathan and S. Chandrasekar, “Pattern Formation on Free Surfaces by Plastic Buckling and Folding,” *Euro Physics Letters*, 129 (2020) 46001. doi: 10.1209/0295-5075/129/46001, 2020

9. T. Sugihara, A. Udupa, K. Viswanathan J. M. Davis, and S. Chandrasekar, “Organic Monolayers Disrupt Plastic Flow in Metals,” *Science Advances*, 6-51, 2020, doi: 10.1126/sciadv.abc8900

10. M. N. Issahaq, S. Chandrasekar, and K. P. Trumble, “Single-Step Shear-Based Deformation Processing of Electrical Conductor Wires,” *J. Manuf. Sci. Eng.*, vol. 143, no. 5, 2021, doi: 10.1115/1.4048984.

11. M. Saei, Mechanics of Ductile Fracture and Segmented Chip Formation in Cutting of Metals, PhD Thesis, Purdue University, May 2021.

12. Poster: B. S. Puentes, J. B. Mann and S. Chandrasekar; Poster: “Hybrid Cutting-Extrusion for Sheet Metal Production with Exceptional Microstructure Control,” TMS 2022 Annual Meeting, Anaheim, CA, 27-3 March 2022. Stiven Puentes won the TMS Materials Processing and Manufacturing Division Graduate Student Poster Competition.

13. A. Udupa, T. Sugihara, K. Viswanathan, R. M. Latanision, and S. Chandrasekar, “Surface-Stress Induced Embrittlement of Metals,” *ACS Nano Letters,* 2021, https://doi.org/10.1021/acs.nanolett.1c02887

14. M. N. Issahaq, A. Udupa, M. Saei, D. P. Mohanty, J. B. Mann, N. K. Sundaram, K. P. Trumble and S. Chandrasekar, Dual-scale folding in cutting of commercially pure aluminum alloys,” International Journal of Machine Tools and Manufacture, 181 (2022) 103932. doi: 10.1016/j.ijmachtools.2022.103932.

15. B. S. Puentes Rodriguez, High-Resistivity Electrical Steel Thin Strip by Hybrid Deformation Processing, PhD Thesis, Purdue University, August 2022.

16. A. Udupa, N. K. Sundaram, A. Mahato, T.Sugihara, J. B. Mann, and S.Chandrasekar, “What Can Plastic Flow Fields Tell Us About Heat Sources In Deformation Processing?,” Journal of Metals, 2021, https://doi.org/10.1007/s11837-021-05071-5.

17. US Patent Application 17/091,400, Methods of Modifying Material Flow Mode During Machining and Products Formed Thereby, T. Sugihara, S. Chandrasekar, A. Udupa, K. Viswanathan, K. P. Trumble and J. B. Mann Filed November 6, 2020. Published US 2021/0205940 A1, July 8, 2021. Disclosed on iEdison invention report.

11. Bibliography

Section 2

B. S. Puentes Rodriguez, High-Resistivity Electrical Steel Thin Strip by Hybrid Deformation Processing, PhD Thesis, Purdue University, August 2022

D. Dietrich, Magnetically Soft Alloys, in: ASM Handbook, Tenth Edition, Vol. 2, 762 (1990) DOI: 10.31399/asm.hb.v02.a000109

J. Schoen and R. Comstock, "Method of continuous casting non-oriented electrical steel strip," U.S. Patent No. 7,140,417. November 28, 2006.

J. Hong, H. Choi, S. Lee, J. K. Kim, and Y. mo Koo, "Effect of Al content on magnetic properties of Fe-Al Non-oriented electrical steel," *J. Magn. Magn. Mater.*, vol. 439, pp. 343–348, 2017, doi: 10.1016/j.jmmm.2017.03.082.

J. H. Yu *et al.*, "The effect of heat treatments and Si contents on B2 ordering reaction in high-silicon steels," *Mater. Sci. Eng. A*, 2001, doi: 10.1016/S0921-5093(00)01960-2.

K. Narita, N. Teshima, Y. Mori, and M. Enokizono, "Recent researches on high silicon-iron alloys," *IEEE Trans. Magn.*, vol. 17, no. 6, pp. 2857–2862, 1981, doi: 10.1109/TMAG.1981.1061740.

T. Ros, Y. Houbaert, O. Fischer, and J. Schneider, "Thermomechanical processing of high Si-steel (up to 6.3% Si)," *IEEE Trans. Magn.*, vol. 37, no. 4, pp. 2321–2324, 2001, doi: 10.1109/20.951160.

J. Stodolny and J. Groyecki, "Cold deformability of Fe-Si-Al alloys," *Phys. Scr.*, vol. 39, no. 2, pp. 279–281, 1989, doi: 10.1088/0031-8949/39/2/017.

B. S. Puentes Rodriguez, D. Brice, J. B. Mann, S. Chandrasekar, and K. Trumble, "Production of High-Resistivity Electrical Steel Alloys by Substitution of Si with Al and Cr," in *TMS 2019 148th Annual Meeting & Exhibition Supplemental Proceedings*, 2019, pp. 599–606.

G. Ouyang, X. Chen, Y. Liang, C. Macziewski, and J. Cui, "Review of Fe-6.5 wt%Si high silicon steel—A promising soft magnetic material for sub-kHz application," *Journal of Magnetism and Magnetic Materials*, vol. 481. pp. 234–250, 2019, doi: 10.1016/j.jmmm.2019.02.089.

V. Mânescu, G. Pâltânea, and H. Gavrilâ, "Non-Oriented Silicon Iron Alloys – State of the Art and Challenges," *Rev. Roum. Sci. Techn.-Electrotechn. Energ.*, vol. 59, pp. 371–380, 2014, doi:

10.5923/j.eee.20120206.07.

M. Littmann, “Iron and silicon-iron alloys,” *IEEE Trans. Magn.*, vol. 7, no. 1, pp. 48–60, 1971, doi: 10.1109/TMAG.1971.1066998.

M. Komatsubara, K. Sadahiro, O. Kondo, T. Takamiya, and A. Honda, “Newly developed electrical steel for high-frequency use,” *J. Magn. Magn. Mater.*, vol. 242–245, pp. 212–215, 2002, doi: 10.1016/S0304-8853(01)01164-7.

P. A. Beck and P. R. Sperry, “Strain induced grain boundary migration in high purity aluminum,” *J. Appl. Phys.*, vol. 21, no. 2, pp. 150–152, 1950, doi: 10.1063/1.1699614.

J. C. Perrier and P. Brissonneau, “Some physical and mechanical properties of SiAlFe alloys,” *J. Magn. Magn. Mater.*, vol. 26, pp. 79–82, 1982, doi: https://doi.org/10.1016/0304-8853(82)90121-4.

G. Langford, P. K. Nagata, R. J. Sober, and W. C. Leslie, “Plastic Flow in Binary Substitutional Alloys of BCC Iron-Effects of Wire Drawing and Alloys Content on Work Hardening and Ductility,” *Metall. Mater. Trans.*, vol. 3, no. 7, pp. 1843–1849, 1972, doi: 10.1007/BF02642569.

A. B. Kustas, “Shear-Based Deformation Processing and Characterization of Electrical Steel Sheet,” no. Open Access Dissertations. 1241., p. 161, 2016, [Online]. Available: https://docs.lib.purdue.edu/open_access_dissertations/1241.

G. Lyudkovsky, P. K. Rastogi, and M. Bala, “Nonoriented Electrical Steels,” *JOM*, vol. 38, no. 1, pp. 18–26, 1986, doi: https://doi.org/10.1007/BF03257950.

V. Mânescu, G. Pâltânea, and H. Gavrilâ, “Non-Oriented Silicon Iron Alloys – State of the Art and Challenges,” *Rev. Roum. Sci. Techn.-Electrotechn. Energ.*, vol. 59, pp. 371–380, 2014, doi: 10.5923/j.eee.20120206.07.

F. E. Werner and R. I. Jaffee, “Energy-efficient steels for motor laminations,” *J. Mater. Eng. Perform.*, vol. 1, no. 2, pp. 227–234, 1992, doi: 10.1007/BF02648621.

Section 3

S. Molafilabi, A. Sadeghi, and M. Hadad, “Investigation of large strain extrusion machining (LSEM) of pure magnesium (Mg),” *Int. J. Light. Mater. Manuf.*, vol. 3, no. 2, pp. 100–107, 2020, doi: 10.1016/j.ijlmm.2019.09.001.

A. B. Kustas, D. R. Johnson, K. P. Trumble, and S. Chandrasekar, “Enhancing workability in sheet production of high silicon content electrical steel through large shear deformation,” *J. Mater. Process. Technol.*, vol. 257, no. February, pp. 155–162, 2018, doi: 10.1016/j.jmatprotec.2018.02.027.

D. Sagapuram, M. Efe, K. P. Trumble, and S. Chandrasekar, “Enabling shear textures and fine-

grained structures in Magnesium sheet by machining-based deformation processing," *IOP Conf. Ser. Mater. Sci. Eng.*, vol. 63, no. 1, pp. 0–10, 2014, doi: 10.1088/1757-899X/63/1/012155.

W. Moscoso, M. R. Shankar, J. B. Mann, W. D. Compton, and S. Chandrasekar, "Bulk nanostructured materials by large strain extrusion machining," *J. Mater. Res.*, vol. 22, no. 1, pp. 201–205, 2007, doi: 10.1557/jmr.2007.0021.

T. L. Brown *et al.*, "A study of the interactive effects of strain, strain rate and temperature in severe plastic deformation of copper," *Acta Mater.*, vol. 57, no. 18, pp. 5491–5500, 2009, doi: 10.1016/j.actamat.2009.07.052.

R. L. Brown, "Strip Fabrication Using Peeling Techniques," *Mater. Manuf. Process.*, vol. 4, no. 4, pp. 467–481, 1989, doi: 10.1080/10426918908956310.

A. Middlemiss, D. Hague, and M. C. Gleave, "Strip production by peeling," *Met. Technol.*, vol. 9, no. 1, pp. 413–418, 1982, doi: 10.1179/030716982803286322.

Section 4

M. Saei, Mechanics of Ductile Fracture and Segmented Chip Formation in Cutting of Metals, PhD Thesis, Purdue University, May 2021.

Section 5

G. Bertotti, A. Canova, M. Chiampi, D. Chiarabaglio, F. Fiorillo, and A. M. Rietto, "Core loss prediction combining physical models with numerical field analysis," *J. Magn. Magn. Mater.*, vol. 133, no. 1, pp. 647–650, 1994, doi: 10.1016/0304-8853(94)90646-7.

W. A. Pluta, "Some properties of factors of specific total loss components in electrical steel," *IEEE Trans. Magn.*, vol. 46, no. 2, pp. 322–325, 2010, doi: 10.1109/TMAG.2009.2033559.

J. F. Gieras, *Advancements in Electric Machines,* Chapter 2, Materials Engineering, 1st ed. 20. Dordrecht: Springer Netherlands, 2008.

E. T. Stephenson, "Effects of thickness and resistivity on core loss and permeability of nonoriented semiprocessed steels," *J. Appl. Phys.*, vol. 55, no. 6, pp. 2142–2144, 1984, doi: 10.1063/1.333590.

G. Bertotti, "General Properties of Power Losses in Soft Ferromagnetic Materials.," *IEEE Trans. Magn.*, vol. 24, no. 1, pp. 621–630, 1987, doi: 10.1109/20.43994.

G. Bertotti, D. Chiarabaglio, F. Fiorillo, A. Boglietti, M. Chiampi, and M. Lazzari, "An improved estimation of iron losses in rotating electrical machines," *IEEE Trans. Magn.*, vol. 27, no. 6, pp. 5007–5009, 1991, doi: 10.1109/20.278722.

ASTM A773-21 Standard Test Method for Direct Current Magnetic Properties of Low Coercivity Magnetic Materials Using Hysteresis Graphs, ASTM International (2021).

ASTM A927-18 Standard Test Method for Alternating-Current Magnetic Properties of Toroidal Core Specimens Using the Voltmeter-Ammeter-Wattmeter Method, ASTM International (2018).

H. Zhao *et al.*, "An Improved Core Loss Model of Ferromagnetic Materials Considering High-Frequency and Nonsinusoidal Supply," *IEEE Trans. Ind. Appl.*, vol. 57, no. 4, pp. 4336–4346, 2021, doi: 10.1109/IAS44978.2020.9334779.

Development of New Steel Alloy to Reduce Core Losses in Electric Motors, US DOE Office of Energy Efficiency and Renewable Energy, Advanced Manufacturing Office, DOE/EE-1578 Project Highlight, November 2017.

Section 6

R. J. Fruehan, O. Fortini, H. W. Paxton and R. Brindle, Theoretical minimum energies to produce steel for selected conditions; Report for the US Department of Energy, Office of Industrial Technology (2000).

Y. Sakamoto, Y. Tonooka, and Y. Yanagisawa, Estimation of energy consumption for each process in the Japanese steel industry, Energy Conservation and Management, 40, 1129-1140 (1999).

G. E. Dieter, Mechanical Metallurgy, McGraw-Hill, 3rd Ed, (1986).

J. A. Schey, Introduction to Manufacturing Processes, Mc-Graw-Hill, 2nd Ed, (1987).

Section 7

Cogent Power NO18 data. https://cogent-power.com/cms-data/downloads/Hi-Lite_NO18.pdf

ASTM Standard E290-14 Standard Test Methods for Bend Testing of Material for Ductility, ASTM International, 2014.

V. Burt, "Forming of Aluminum Alloys," *ASM Handbook, Volume 2A, Aluminum Science and Technology*, 2018.

Custom Part Net. https://www.custompartnet.com/wu/sheet-metal-shearing

H.M.S. Harstick, M. Ritter, W. Riehemann, "Influence of Punching and Tool Wear on the Magnetic Properties of Nonoriented Electrical Steel," *IEEE Transactions on Magnetics*, v50, 6200304, 2014.

Bending of Sheet Metal, ASM Handbook, Volume 14B: Metalworking: Sheet Forming (Editor: S.L. Semiatin), ASM International, 2006.

Cogent Power General Brochure https://dennisfurlancom.files.wordpress.com/2017/01/cogent-brochure-final.pdf